



Moisture availability and productivity at Lake Nakuru, Kenya leading into the African Humid Period

Elena Robakiewicz ^{a,b,c,*}, Andreas G.N. Bergner ^d, Carolina Rosca ^e, Simon Kübler ^f, Veronika Ketzer ^c, Martin H. Trauth ^g, Annett Junginger ^{c,h}

^a University of Cologne, Institute for Geography Education, Cologne, Germany

^b University of Connecticut, Storrs, CT, USA

^c Eberhard Karls University Tübingen, Department of Geosciences, Tübingen, Germany

^d GFZ Helmholtz Centre for Geosciences, Potsdam, Germany

^e Andalusian Earth Sciences Institute (IACT-CSIC), Armilla, Granada, Spain

^f LMU Munich, Department of Earth and Environmental Sciences, Munich, Germany

^g University of Potsdam, Institute of Geosciences, Potsdam, Germany

^h Senckenberg Centre for Human Evolution and Paleoenvironment (SHEP), Tübingen, Germany

ARTICLE INFO

Handling editor: Mira Matthews

Keywords:

Paleohydrology

Diatoms

Anoxia

Geochemistry

Heinrich events

μ -XRF

ABSTRACT

Lake Nakuru, a lake with one of the highest primary production rates in the world, is an eastern African soda lake that contains important records of environmental change since the Late Pleistocene. As a closed basin at one of the highest points of the East African Rift System, Lake Nakuru shows significant changes in lake level from annual to millennial timescales even during times of minor precipitation change. Various studies have focused on Lake Nakuru in part due to abundant archaeological sites within the surrounding basin. Despite research attention focused on Nakuru's record related to rift-wide environmental reconstructions across the East African Rift System, little focus has been made on its own unique sedimentary record. Here we present a new multi-proxy record from the upper ~11.5 m of two duplicate 17-m drill cores from Lake Nakuru. Using lithological, diatom, total nitrogen, total carbon, total organic carbon, and micro-X-ray fluorescence data with a multi-annual to decadal time resolution, we provide insights into lake depth and hydroclimatic changes of the past 35,000 years. The available age model indicates recurring anoxic phases based on μ -XRF and lithological data coeval with low diatom species richness and abundant *Thalassiosira rudolfi* ~35, ~25.5 to 24.5, and 19.5 to 17.5 ka. *T. rudolfi* therefore acts as an indicator of highly productive and/or deeper waters with limited mixing rather than of higher conductivity/pH, strictly due to increased evaporation within the basin. This indicates the challenge of *T. rudolfi*'s use within highly alkaline soda lakes like Lake Nakuru. Other lake phases evident through this record include dry, shallow conditions from 24.5 to 19.5 ka, alkaline conditions from 17.5 to 15.4 ka, and a variable deepening phase from 15.4 to 13.6 ka followed by a more stable deep phase from 13.6 to 12.6 ka. We propose that hydroclimate changes at Lake Nakuru during this time, including presumed wet, anoxic phases, may be related to high and low latitude teleconnections in sea surface temperatures and moisture availability over the Late Pleistocene.

1. Introduction and research history

Over several decades, scientists have attempted to understand how the hydrological cycle in the African tropics responds to changes in orbital parameters and global climate across the Quaternary. One of the best-studied examples, the African Humid Period (AHP; 15–5 ka)

resulted in a dramatic rise in lake levels across the northern and eastern part of the African continent as the result of a maximum Northern Hemisphere solar radiation during a minimum in orbital precession (e.g., Kutzbach and Street-Perrott, 1985; deMenocal et al., 2000; Shanahan et al., 2015; Tierney and deMenocal, 2013). Despite the well-studied AHP, the controls on other hydrological changes throughout the

* Corresponding author. University of Cologne, Institute for Geography Education, Cologne, Germany.

E-mail address: erobakie@uni-koeln.de (E. Robakiewicz).

Pleistocene are not as well understood (e.g., [Singarayer and Burrough, 2015](#); [Duesing et al., 2021](#); [Lupien et al., 2022](#); [O'Mara et al., 2022](#)). Proxy-based records during the Last Glacial Maximum (LGM; 26–19 ka) and the lead up to the AHP are far more limited due to the dry conditions evident in records from the LGM across northern and eastern Africa ([Gasse, 2000](#); [Gasse et al., 2008](#); [Barker et al., 2004](#); [Shakun and Carlson, 2010](#)). Decreased insolation resulting in decreased latitudinal variability in the mean annual position of the tropical rainbelt ([Kutzbach and Street-Perrott, 1985](#); [Braconnot et al., 2008](#); [Nicholson, 2018](#)) and the expansion of the Northern Hemisphere continental ice sheet ([Arbuszewski et al., 2013](#); [Broecker and Putname, 2013](#)) would reduce eastern African rainfall during the LGM. Yet, these mechanisms cannot accommodate southeastern African LGM records which show in-phase conditions to those from eastern Africa ([Tierney et al., 2008](#); [Stager et al., 2011](#); [Truc et al., 2013](#); [Chase et al., 2022](#)). It has been suggested that low-amplitude precessional variability of the LGM decreases insolation's control on eastern African climate, resulting in other forcing mechanisms increasing in importance ([Trauth et al., 2003](#); [Tjallingii et al., 2008](#); [Kuechler et al., 2013](#); [Singarayer and Burrough, 2015](#)). Controls like sea surface temperatures (SST) of the Indian Ocean ([Tierney et al., 2008](#)), Walker Circulation weakening the El Niño–Southern Oscillation (ENSO) system ([Tian and Jiang, 2020](#)), or a reduction of meltwater suppressing Atlantic Meridional Overturning Circulation (AMOC) ([Otto-Bliesner et al., 2014](#)) (such as during a Heinrich event) have been proposed as controls to reduce rainfall in eastern Africa, but limited records muffle clarity on the LGM's impact on the eastern African tropics.

As a closed basin at one of the highest points of the Eastern African Rift System (EARS) and only 40 km south of the Equator, Lake Nakuru is a valuable site to study past rainfall patterns in the equatorial EARS ([Fig. 1](#)). As a lake with one of the highest primary productivity rates in the world ([Livingstone and Melack, 1984](#); [Vareschi and Jacobs, 1985](#); [Ballot et al., 2004](#)), Lake Nakuru has been the focus of many studies related to Late Pleistocene paleolimnological and paleoclimatological change (e.g., [Leakey, 1931](#); [Nilsson, 1931](#); [Nilsson, 1940](#); [Gregory, 1968](#); [Washbourn-Kamau, 1971](#); [Butzer et al., 1972](#); [Cohen et al., 1983](#); [Hastenrath and Kutzbach, 1983](#); [Cohen and Nielsen, 1986](#); [Dühnforth et al., 2006](#)). Early observations of paleoshorelines, lake deposits, and modern decadal-scale lake level changes ([Nilsson, 1931](#); [Flint, 1959a](#); [McCall, 1967](#)) indicate that as a closed basin with flat basin floor morphology and steep slopes, Lake Nakuru responds sensitively to even minor changes in precipitation ([Nilsson, 1931](#); [Flint, 1959b](#); [Trauth et al., 2010](#); [Olaka et al., 2010](#)).

The Nakuru record was instrumental in understanding African climate change based on [Leakey's \(1931\)](#) and [Nilsson's \(1931\)](#) glacial “Great Pluvial” or “Gamblian” hypothesis. This hypothesis dominated paleoanthropological and archaeological interpretations for decades, claiming that eastern Africa went through periodic wet phases during ice ages (e.g., [Leakey et al., 1943](#); [Leakey, 1950](#); [Cole, 1963](#); [Robson, 1967](#)), which has since been discredited, as summarized by [Kingston and Hill \(2005\)](#). Given the vast abundance of archaeological material in the region observed since the first European explorations ([Gregory, 1921](#)), an interest in the relationship between past climates and hominin evolution and archaeology has driven, and continues to drive, research across the EARS ([Ambrose, 1984](#); [Ambrose and Sikes, 1991](#); [Maslin and Trauth, 2009](#); [deMenocal, 1995](#); [Potts, 1998](#); [Trauth et al., 2010](#); [Griffith, 2020](#); [Foerster et al., 2022](#)).

As scientists were better able to calculate elevation and absolute dates of paleoshorelines, “Gamblian” stratigraphic correlation was abandoned ([Flint, 1959a](#)) and a wealth of understanding was gained regarding past lake levels at Nakuru ([Washbourn-Kamau, 1971](#); [Butzer](#)

[et al., 1972](#)). Micropaleontological evidence (including ostracods and diatoms) from cores taken in 1969 from Lakes Nakuru, Elmenteita, and Naivasha indicate a potential peak in lake levels >24 ka,¹ low lake levels until ~15.5 ka, and a huge increase in lake levels ~11.5 ka ([Cohen et al., 1983](#); [Cohen and Nielsen, 1986](#); [Richardson and Dussinger, 1986](#)). The calculated lake levels from paleoshorelines reveal that a merged Paleolake Nakuru-Elmenteita was 180 m deeper ~11.5 ka than at present ([Fig. 1](#); [Washbourn-Kamau, 1971](#); [Dühnforth et al., 2006](#)). Initial hydro-balance models calculated an increase in precipitation of ~65% during the ~11.5 ka highstand ([Butzer et al., 1972](#); [Richardson and Richardson, 1972](#)), but refined models show that a ~23–45% increase in precipitation is sufficient to produce the AHP highstand due to Lake Nakuru's sensitivity to increased moisture ([Hastenrath and Kutzbach, 1983](#); [Bergner et al., 2003](#); [Dühnforth et al., 2006](#); [Kniess, 2006](#); [Junginger and Trauth, 2013](#)). Despite several previous studies, changes at Lake Nakuru before the AHP are unclear, requiring further evaluation to understand how local environments change in response to global climate.

In this study, a drill core record from Lake Nakuru highlights variability in eastern African hydroclimate before the AHP. Using a multi-proxy record from lithological, micropaleontological, and geochemical data, this paper presents high-resolution (multi-annual to decadal) hydroclimatic change with the aim to explore: (1) How variable is the chemistry, depth, and rate of change of Lake Nakuru at the end of the Pleistocene? and (2) Which aspects of global climate can account for these changes at Lake Nakuru before the AHP? Through a review of other eastern African lake records, we aim to better understand hydroclimate variability from ~35 ka until the AHP. By reconstructing Lake Nakuru's changing depth and productivity over the last 35 kyr, we provide an important overview into environmental changes and cycles across Late Pleistocene-Holocene climatological phases.

2. Geological and modern setting

2.1. Geological setting

Lake Nakuru (00°22'S, 36°05'E; 1760 m above sea level (m asl)) and the neighboring Lake Elmenteita (00°26'S, 36°15'E; 1776 m asl) are located along the highest section of the Kenya Rift in the Eastern Branch of the EARS ([Fig. 1](#); [Renaut and Owen, 2023](#)). The wider region around Nakuru exhibits classic features of an asymmetric rift. Progressively uplifted flanks reach heights of ~2500 m asl in the Kingangop-Bahati Platform, ~4000 m asl in the easterly Aberdare Range, and ~3000 m asl in the westerly Mau escarpment ([McCall, 1967](#)). The central basin floor is ~1800 m asl and is characterized by ongoing faulting and volcanic activity. Rifting in the area aligns along a NNW–SSE axis and was active 12–6 Ma during the late Miocene, with additional activity 5.5–3.7 Ma and ~2.6 Ma, forming a ~40-km-wide inner rift depression ([Baker et al., 1988](#); [Baker and Wohlenberg, 1971](#); [Clarke et al., 1990](#); [Kanda, 2010](#); [McCall, 1967](#); [Roessner and Strecker, 1997](#); [Strecker et al., 1990](#)).

The rift floor has subsequently been covered by trachytic, basaltic, and rhyolitic lavas and tuffs, which have been displaced by normal faulting along a central axis ([McCall, 1967](#); [Clarke et al., 1990](#); [Strecker et al., 1990](#)). During the Middle Pleistocene, a shift in the direction of extension resulted in the development of NNE striking normal faults linked by complex transfer zones with reactivation of some older faults ([Bosworth and Strecker, 1997](#); [Strecker et al., 1990](#); [Zielke and Strecker, 2009](#)). The younger structures in the inner rift are accompanied by Late Pleistocene to Holocene volcanoes, including Menengai, Eburru, and Longonot, as well as smaller rhyolitic domes and basaltic lava flows. Consequently, the present-day inner rift has become compartmentalized

¹ All ages from past studies before 1998 in this paper are calibrated using the RCarbon package in R ([Crema and Bevan, 2021](#)) with INTCAL20 ([Reimer et al., 2020](#)).

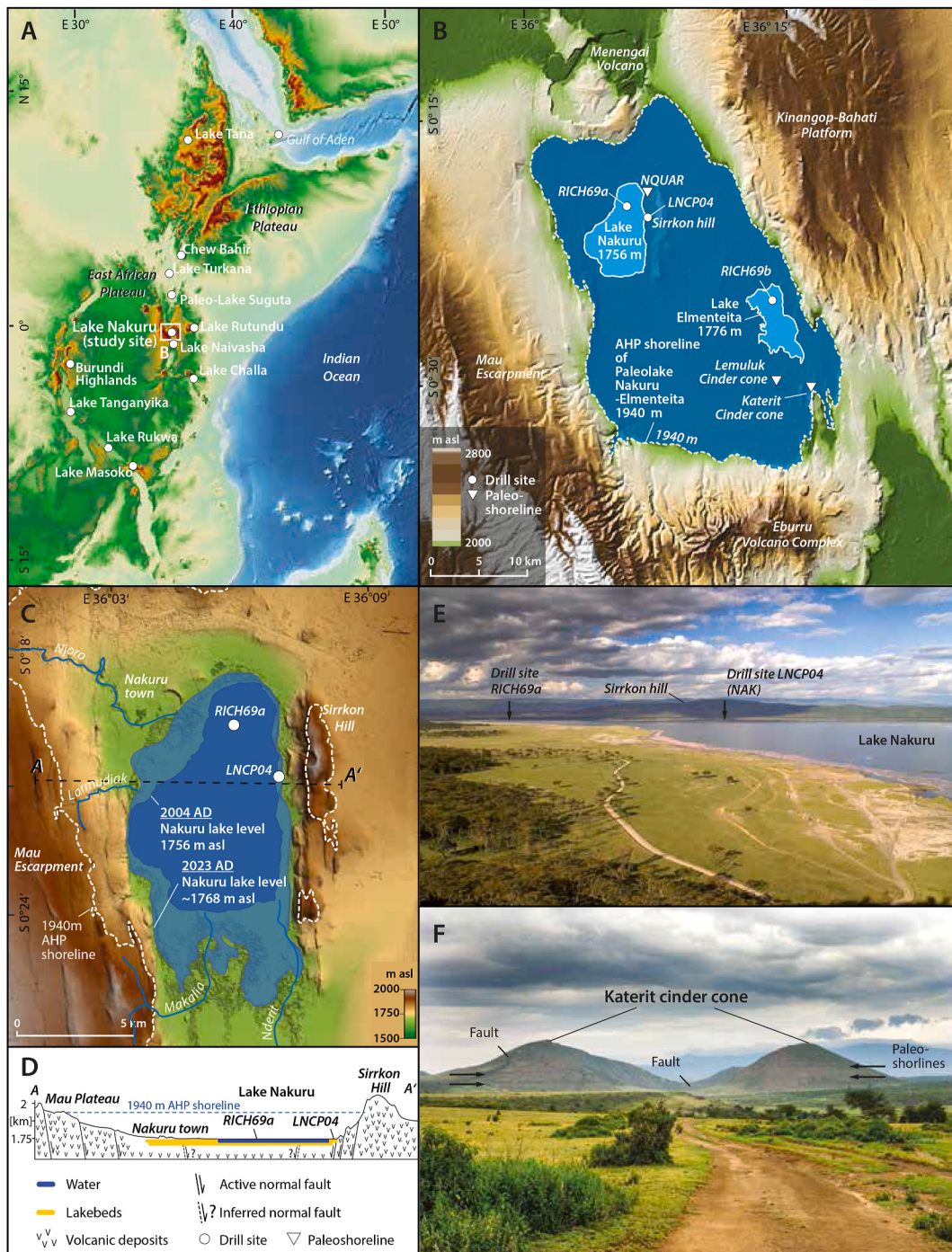


Fig. 1. A) Map of the Kenyan Eastern Branch of the East African Rift System with other basins and lakes discussed in the text labeled and Nakuru highlighted with a box. B) Topographic map of the Nakuru-Elmenteita Basin with the modern lake levels in light blue and the African Humid Period (AHP) highstand at 1940 m above sea level in dark blue (Washbourn-Kamau, 1971). LNCP04 is the core from this study. RICH69a&B are the cores studied by Cohen and Nielsen (1986) and Richardson and Dussinger (1986). C) The modern Nakuru basin with the lake level from 2004 in dark blue, the lake level from 2023 in light blue, and the AHP shoreline dashed white. The Nakuru cores from Richardson and Dussinger (1986) and this study are labeled. D) A cross section from A to A' is used to highlight Sirrkon Hill and the location of nearby faults. The location of the cores and the height of the AHP shoreline are indicated. E) Birds-eye view from 2004 of Nakuru Lake in the direction of Sirrkon Hill with the location of the cores labeled. F) View of the Katerit cinder cone where AHP shorelines are evident. (For interpretation of the references to color in this figure legend, the reader is referred to the Web version of this article.)

into smaller lake basins, primarily the Nakuru-Elmenteita and Naivasha basins, separated by normal faults and intervening volcanic structures (Baker, 1986; Dühnforth et al., 2006; Kübler et al., 2016).

Faulting in the Holocene, particularly toward the middle of the basin, resulted in a N-S striking rift zone and is associated with the most recent volcanic activity (Baker, 1986). One of the basin's most recently dated

fault structures originates from the small volcanoes at the southern shores of Lake Elmenteita. The highest shoreline at Katerit volcano (Fig. 1B and F), dated to 10.2–11.8 ka BP (~180 m above the modern lake level), is associated with the AHP highstand and has been displaced by a normal fault by 2.5 m (Dühnforth et al., 2006).

Menengai, Lake Nakuru's most proximal volcano, initiated ~180 ka,

creating a physical barrier to the north separating the Nakuru-Elmenteita basin from the Baringo-Bogoria basin (McCall, 1967; Leat, 1984). The Menengai Tuff dated to 35.62 ± 0.26 ka is a standard marker across the EARS, given its spread of over $115,000 \text{ km}^2$ (Blegen et al., 2016). Eburru, a dissected volcanic massif that formed <450 ka (Clarke et al., 1990) separates the Nakuru-Elmenteita basin from the Naivasha basin in the south (McCall, 1967).

Our study site is located at the foot of a dissected Late Pleistocene trachytic volcanic complex called Sirrkon (or Lion) Hill (Fig. 1C and D; Conti et al., 2021). The volcanic material of the Nakuru-Elmenteita Basin consists of peralkaline or metaluminous trachyte or sodium- and carbonate-rich pantellerite which, in addition to semi-arid conditions, leads to the alkaline nature of modern-day Lake Nakuru (Baker and Wohlenberg, 1971; Leat, 1984). Exposed rocks in the basin consist of either volcanics (including lavas, ashes, tuffs, and pumices) or sediments (including alluvial/colluvial sands and silts; diatomites and diatomaceous silts; and pebble beds) (Conti et al., 2021), highlighting previous phases in which the basin was far wetter. Given the high elevation of Lake Nakuru which limits outside input into the basin, local geology has strong control on the hydrochemistry of the lake.

2.2. Modern hydrological setting

The amount of rainfall in equatorial eastern Africa is controlled by changes in sea surface temperatures (SST) and by the complex tectonic structure of the rift itself (Nicholson, 1996). During positive Indian Ocean Dipole years, SST warm in the western Indian Ocean and cool in the eastern Indian Ocean, weakening Walker Circulation and increasing eastern African rainfall (Marchant et al., 2007; Hiron and Turner, 2018; Lüdecke et al., 2021). SST in the Pacific Ocean impact eastern African rainfall through El Niño Southern Oscillation (ENSO) where warm SST in the eastern Pacific and cool SST in the western Pacific yield heavier rainfall over equatorial eastern Africa, particularly during the short rains (Nicholson, 1996, 2017; Ntale and Gan, 2004). SST also impact the strength of the West African and Indian monsoons, which create dry conditions over eastern Africa during the monsoon season, but wetter conditions off-season (Nicholson, 1996, 2017). The complex topography across the EARS causes local variation in rainfall as local highlands can block moist airflow (Nicholson, 1996). Beyond these factors, variability may also be dependent on North Atlantic Oscillation, Atlantic Multi-decadal Oscillation, and volcanic activity, although these factors are less important and/or less understood (Lüdecke et al., 2021).

Lake Nakuru has a mostly closed drainage system that covers 1475 km^2 with no surface outflow, meaning that outflow is mostly controlled by evaporation and subsurface seepage (McCall, 1967; Milbrink, 1977; Odada et al., 2006; Jirsa et al., 2013; Herrnegger et al., 2021). As a mostly closed system, water budget input is controlled almost exclusively by local climate, with inflow controlled by precipitation, the perennial Ngosur River, and local ephemeral rivers (Makalia, Nderit, Njoro, and Larmudiac) (Fig. 1C; Odada et al., 2006; Kimaru et al., 2019). Input from the rivers is minimal, however, because the sediments below are porous and water is often lost through fissures (McCall, 1967). In contrast to other lakes within the EARS, Lake Nakuru does not have modern groundwater inflow from hot springs through local faults (Odada et al., 2006; Jirsa et al., 2013). With most of the inflow and outflow controlled by the ratio between precipitation and evaporation, Nakuru is an amplifier lake – a lake that responds sensitively to small changes in climate (Olaka et al., 2010). This is evident over the past 100 years of recorded lake levels which show high variability (Washbourn-Kamau, 1971; Odada et al., 2006; Kimaru et al., 2019; Renaut and Owen, 2023). Current increased flood intensity began in 2009 and is likely linked to modern anthropogenically-influenced climate (Fig. 1C; RCMRD, 2021).

Today, Lake Nakuru is a semi-arid environment where annual rainfall varies between 700 and 900 mm/yr, with annual evaporation $\sim 1800 \text{ mm/yr}$ (Odada et al., 2006; Jirsa et al., 2013). The lake receives

rainfall twice a year due to the annual latitudinal migration of the tropical rain belt causing long rains from March to May and short rains from October to November (Nicholson, 1996, 2017). While the tropical rain belt attracts moisture through large-scale advection from the Indian Ocean (Levin et al., 2009), the humid south-westerly Congo Air stream, sourced from the Atlantic Ocean, delivers additional rainfall to the western parts of equatorial eastern Africa in August/September known as the “September rains” (Nicholson, 1996; Camberlin, 1997). The Congo Air Boundary (CAB) separates the western humid airmasses from the eastern dry airmasses causing Nakuru to not be influenced by the September rains. While the CAB does not influence rainfall in the Nakuru-Elmenteita basin today, changes in the Earth’s precession and associated solar insolation on a scale of thousands of years may have resulted in the CAB’s north-eastward expansion and thus influencing the Nakuru region (Junginger et al., 2014). Over the past decade, the surface area of Lake Nakuru has varied between 52 and 65 km^2 (RCMRD, 2021), with an average historical low between 0.5 and 3.5 m (Jirsa et al., 2013). Because of its shallow depth, Lake Nakuru is only temporarily thermally stratified in the middle of the day, with winds mixing the lake in the afternoon, resulting in high primary productivity and the largest population of lesser flamingos in the world (Vareschi and Jacobs, 1985). As a result of local peralkaline trachytes and high evaporation, the lake is highly alkaline and saline of the $\text{Na}-\text{HCO}_3$ -type. More information about modern Lake Nakuru can be found in the recent summary by Renaut and Owen (2023).

3. Material and methods

3.1. Core collection and composite

Cores NAK-X and NAK-Y were collected during the Lake Naivasha/Nakuru Coring Project (LNCP) in 2004 – 15 m apart in overlapping sections with a Usinger Coring System. The coring site is located on the eastern shore of Lake Nakuru in Kenya ($-0.345925, 36.115342$; Fig. 1) and was above water during collection. Sixteen meters were collected for NAK-X and 17 m for NAK-Y (Suppl. 1). This study focuses on a ~ 11.5 m composite section (NAK) representing the first ~ 7 m of NAK-X and the overlapping ~ 10.5 m of NAK-Y (Fig. 2). The cores were split at the Geoforschungszentrum Potsdam (GFZ) in Germany and are currently located at Eberhard Karls Universität Tübingen. The NAK core composite was created using LacCore CoreWall programs based on original photographs, μ -X-Ray Fluorescence (μ -XRF) data, magnetic susceptibility (MagSus), and recent core photo scans. Data were then spliced and converted into the composite using CoreWall and Feldman.

3.2. Chronology

Thirteen organic samples (paleoroots, charcoal) were collected and wet sieved from NAK-Y and NAK-X for radiocarbon dating and two tephra samples for $^{40}\text{Ar}/^{39}\text{Ar}$ dating (Table 1, Fig. 2). Pieces of charcoal or paleoroots larger than $250\text{-}\mu\text{m}$ were picked and sent to Beta analytics, Kiel, and ETH Zürich dating laboratories. Tephra samples were dated at the Berkeley Geochronology Center.

A Bayesian age model was created using the BACON package in R (Blaauw and Christen, 2011) and is accessible in Zenodo. The top of the core was assumed to be modern, given short-term fluctuations in lake level that would cause modern deposition. An additional age from the Menegai Tuff (35.62 ± 0.26 ka, Blegen et al., 2016) was also used given the clear and large deposition from the nearby volcano at ~ 11.54 m. Hiatuses were observed at the top of the small fault at 1.49 m, a sharp transition from sands to clays at 3.09 m, and at a large gap due to core loss at 7.72 m. A thick *in-situ* tephra (2.88–2.90 m) represents a slump in the age model.

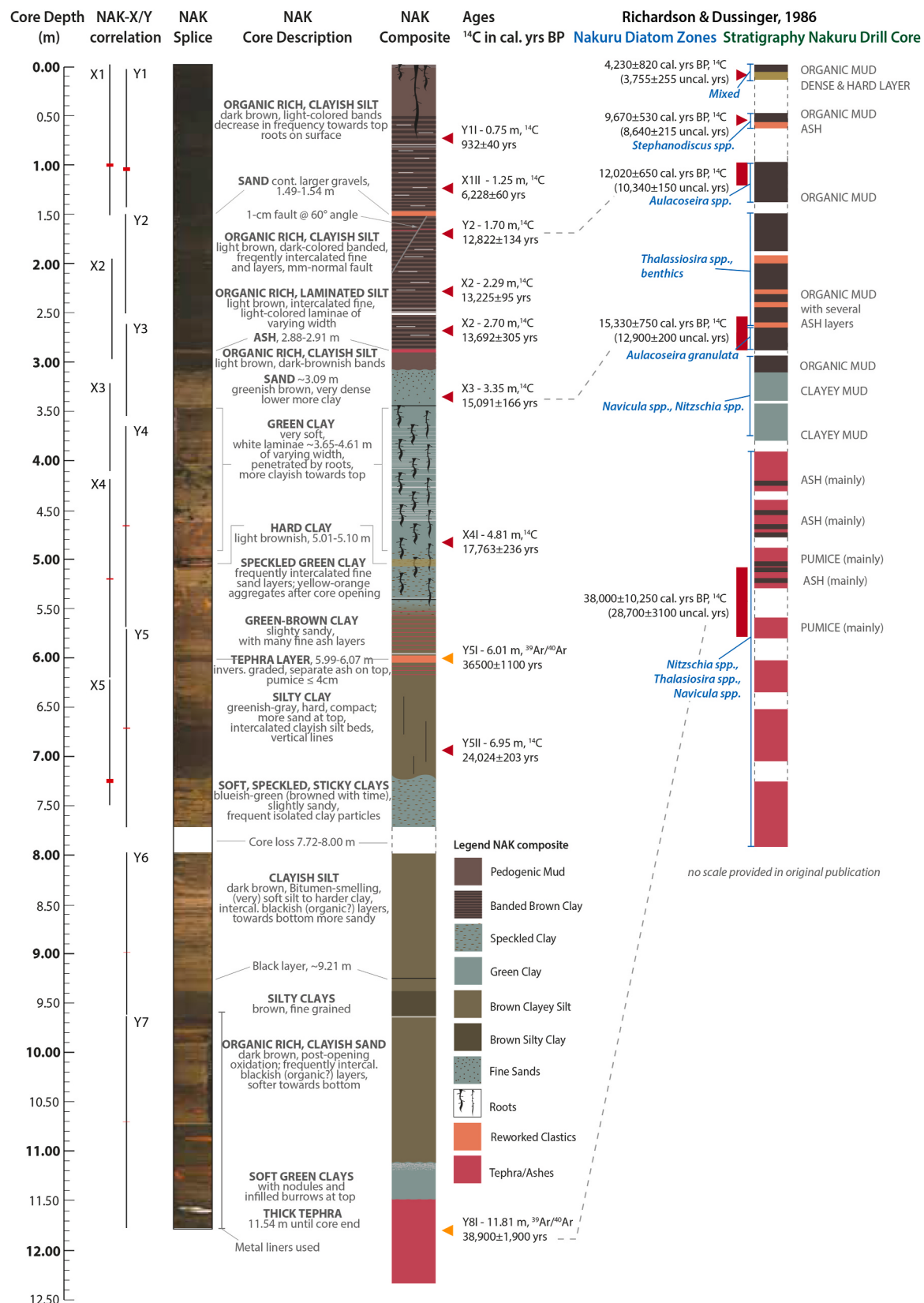


Fig. 2. Stratigraphic columns of core from Nakuru including NAK (this study) and the core from Richardson and Dussinger (1986). Included for NAK are the core correlations, the splice from photos taken in 2019, a detailed core description, and the composite core (NAK) with the ages determined in this study. It is next to the Richardson and Dussinger (1986) core which does not have depth. The ages and their sample areas are included, as well as the observed stratigraphy and diatom zones.

Table 1

Samples used to date the Nakuru cores. Table includes the sample name, the core location, the composite location, the sample type, the uncalibrated ages and their errors, the calibrated median ages and their errors using RCarbon (Crema and Bevan, 2021), and the calibrated median ages and their errors from within the age model (Blaauw and Christen, 2011).

Internal ID	Dating Lab ID	Sample name	Composite Core depth (m)	Sample Type	Uncalibrated age		Calibrated age (cal. BP)		Agemodel (AM) age	
					Uncal. Age [years]	95 % CI [years]	Cal. Median [years]	95 % CI [years]	Cal. Median (AM) [years]	95 % CI (AM) [years]
NAK-AJ-01	Beta-358080	X1I-57.5-62.5	0.6	Charcoal	failed due to too little material	-	-	-	-	-
NAK-AJ-17	Beta-414236	Y1I 68-72	0.75	Charcoal	1020	±30	932	±40	904	-105, +260
NAK-AJ-02	Beta-358081	X1II 18-23	1.25	Charcoal	5400	±30	6228	±60	6066	-144, +195
BER_PDM_NAK-5	KIA 27357	Y2 15-20	1.7	Charcoal	10,925	±45	12,822	±134	12,770	-287, +126
NAK-AJ-03	Beta-358082	X2 28-33	2.29	Charcoal	11,340	±60	13,225	±95	13,226	-238, +173
BER_PDM_NAK-03	KIA 26693	X2 68-73	2.7	Charcoal	11,844	±78	13,692	±305	13,689	-270, +293
BER_PDM_NAK-06	KIA 27358	Y3-37.5-40.0	3.07	Charcoal	failed due to pyrite coating	-	-	-	-	-
BER_PDM_NAK-07	Beta-358083	X3 8-10	3.35	Charcoal	12,660	±50	15,091	±166	15,021	-412, +252
BER_PDM_NAK-08	KIA 27359	X4I 63-71	4.83	Paleoroot	14,545	±55	17,763	±236	17,755	-375, +354
BER_PDM_NAK-10	KIA 27356	X4I-90-94	5.13	Charcoal	failed due to pyrite coating	-	-	-	-	-
60011	Ar01	Y5I-28-30.5	6.01	Tephra	36,500	±1100	-	-	-	-
BER_PDM_NAK-15	Beta-414237	Y5II 19-24	6.95	Charcoal	20,020	±80	24,024	±203	23,934	-470, +282
T111206_2	Ar06	Y8I-30-45	11.81	Tephra	38,900	±1900	-	-	-	-

*The date used for the tephra at the bottom of the section for the age model is from (Blegen et al., 2016) as our deposits are likely the Menengai Tuff and this date is more constrained than the sample taken from NAK.

3.3. Core measurements

3.3.1. Magnetic susceptibility (MagSus)

MagSus was measured for NAK-X and NAK-Y using an automatic Bartington® point sensor with 1-mm point separation and 4-mm spatial resolution at the GFZ. Only 10 m of NAK-X and 9 m of NAK-Y were measured, as metal liners were used beginning at NAK-X8 and NAK-Y7 (Suppl. 2). MagSus data was smoothed using a Triangular Moving Average (filter = 10) using the Zoo Package (Zeileis and Grothendieck, 2005) and plotted using the Rioja Package (Juggins, 2022) in R.

3.3.2. μ -X-Ray fluorescence and Principal Component Analysis (PCA)

μ -XRF scanning was performed at the Max-Planck Institute in Mainz in 2021 with a Avaatech scanner using a rhodium tube and the protocol from Richter et al. (2006). Elements were scanned along 1-mm intervals at 10 kV and/or 30 kV. The scanned elements at 10 kV include Mg, Al, Si, P, S, Cl, Ar, and Ba; at 10 and 30 kV, K, Ca, Ti, V, Cr, Mn, Fe, Co, Ni, and Cu; and at 30 kV, Sc, Zn, Ga, As, Br, Rb, Sr, Y, Zr, Mo, Pb, U, Coherence, and Incoherence (Suppl. 3). The degradation of the metal liners below ~9.6 m impacts the μ -XRF record and should be interpreted with caution. Gaps and inconsistencies in the data were noted and removed using CoreWall. Smoothing using a Triangular Moving Average (filter = 10) was conducted with the Zoo Package (Zeileis and Grothendieck, 2005) and plotted using the Rioja Package (Juggins, 2022) in R.

Principal Component Analysis (PCA) was conducted on the μ -XRF data and run in R using multiple packages which are visible in the code available on Zenodo. Elements with medians <50 counts per second (cps; Mg, P, V, Cr, Cu, Ba, Sc, Ga, As, Br, and Ar (Suppl. 4; 5)) were not included in the PCA. Other removed elements include Cl, which indicated whether NAK-X or NAK-Y were used in the NAK splice, as well as Mn and Zn, which were flat along the core until the metal liners. For elements with μ -XRF data from both the 10 kV and 30 kV runs, 10 kV

results were used as they resulted in higher eigenvalues for the PCA except for Ni where the 10 kV data were <50 cps.

3.3.3. Water content, total nitrogen, total and organic carbon

NAK-Y was sampled at ~10-cm resolution for water content (WC), total carbon (TC), total nitrogen (TN), and total organic carbon (TOC) analysis (Suppl. 6). To determine WC, sample weights were measured before and after freeze-drying. The freeze-dried samples were homogenized using an Agate mortar and analyzed concurrently by IR-spectroscopy and heat conductivity detection after burning weighed aliquots in an oxygen gas flow at 1350 °C using a LECO CNH 2000 Elemental Analyzer (LECO Corp., St. Joseph, MI). Total organic carbon was determined after release of CO₂ by reaction with hot 4% and 25% HCl followed by using the LECO, CNH 2000 system again.

3.4. Diatom analyses

3.4.1. Sampling and counting

Diatom samples (N = 216) were collected every ~5 cm. Samples were prepared using the Battarbee (1986) hot H₂O₂ method. Dry samples, weighed to ~0.1 g, were treated with 30% H₂O₂ to remove organic matter and 10 % HCl to remove carbonates. The samples were then centrifuged at 2500 RPM for 5 minutes and repeatedly decanted. After decanting a third time, a drop of ammonia solution (30–33% NH₃) was added to disaggregate sediments and colonial diatoms. The samples were then centrifuged and decanted twice more. Upon completion, *Lycopodium* microspores (Batch 3862; 9,666 spores) were added to the solution and dissolved to quantify diatom concentration:

$$\text{Diatom Concentration} = \frac{(\# \text{ of Microspores Introduced} * \# \text{ of Counted Diatoms})}{(1 + \# \text{ of Microspores Counted})}$$

Coverslips with prepared sample dried in a dry air ventilator for 24

hours and then adhered to slides using Naphrax and placed on a 125 °C hot plate for 20 minutes. All counts were conducted using an Olympus BX50 light microscope at 1000x magnification with a 700D Canon Camera. 70-nm gold-coated samples were observed using a Phenom XL Scanning Electron Microscope with a Back Scatter Detector with 15 kV acceleration voltage at the Microfossils Laboratory in the Department of Geosciences of Universität Tübingen (electron source, Cerium Hexaborite (CeB₆) cathode). Diatom taxa identification is based on Gasse (1986), Cocquyt (1998), Taylor et al. (2007), Taylor and Cocquyt (2016), the US Diatom Database (Spaulding et al.), and Cocquyt and Verschuren (2023). The majority of diatoms that make up ≥ 5% of one sample are included in a diatom plate in Supplemental 7.

A minimum of 300 diatom valves were counted per slide (Suppl. 8). If one species was dominant, a minimum of 100 non-dominant valves were counted. For analysis, percentages of each taxon relative to the total number of counted valves per sample were calculated. Stratigraphic zones based off of the diatom assemblages were calculated using constrained hierarchical clustering with Bray-Curtis dissimilarity within the Rioja Package in R (Juggins, 2022).

3.4.2. Transfer function

Ecological interpretations are based on modern assemblage data from the East African diatom dataset within the European Diatom Database Index (Battarbee et al., 2001) and were used to interpret conductivity and pH using the weighted averaging method (Suppl. 9; ter Braak and Loaman, 1986; Gasse et al., 1995). Statistical analyses were conducted in R and all stratigraphic plots were made with the package Rioja (Juggins, 2022), available in Zenodo.

3.4.3. Other diatom proxies

Species richness was calculated using the Vegan Package in R (Oksanen et al., 2022). A mixing proxy was calculated using *Aulacoseira*/(*Cyclostephanos* + *Stephanodiscus* + 1) (A/(C + S)), where an increase indicates greater mixing with a strong nutrient flux and high Si:P ratio in the euphotic zone (Gasse et al., 2002). Aerophilic and brackish taxa, based on Gasse (1986) and Taylor et al. (2007), were also plotted to show relative changes across the assemblages (Suppl. 10). Lastly, an index was created to highlight increasing freshness, *Thalassiosira faurii*/(*T. faurii* + *T. rudolfi*) (*T. Index*).² All diatom plots were made with the Rioja Package in R (Juggins, 2022).

4. Results

4.1. Composite lithology and correlation

NAK is dominated by finely laminated clayey silts and clays of different colors and laminae thicknesses (<1–10 mm) with occasional fine sandy sections and tephra (Fig. 2; Suppl. 1). The upper ~0.6 m of the NAK composite are densely rooted, dark-brown, organic-rich pedogenic clayish silts. Below ~0.6 m, banded brown clays are interspersed with mm-thick white diatomaceous layers. After a reworked lapilli/sand layer from 1.49–1.54 m, the banded brown clays continue with a small 1-cm fault offset at a 60° angle to the horizontal plane until ~2.15 m. White, diatom-rich bands become denser from 2.4–2.6 m. These layers are interrupted by an *in-situ* ash 2.88–2.91 m. Below this point, non-laminated organic-rich clayish silts abruptly transition into coarser sands at ~3.09 m. These light gray, greenish sands grade downwards

into finer grain sediments until a black layer at 3.44 m. This black layer marks the beginning of mixed clays with plant remnants, potentially indicating pedogenesis and short-term desiccation. Short roots (several cm-long) from multiple surface horizons continue in the sediments down to ~5.55 m. The clays after 3.44 m are green and unlaminated until ~3.65 m, after which they are well-laminated with white, diatom-rich laminations (<2-mm thick) that thicken until ~4.61 m after which the green clays are unlaminated. At ~4.90 m, the green clays are speckled with yellow-orange sulfur/pyrite aggregates that have formed since core opening in 2004. These continue until the end of the roots at ~5.55 m after which there are many thin ashes across progressively browner clays. A tephra from 5.99–6.07 m was dated to 36.5 ± 1.1 ka (Table 1), indicating reworked sand-sized volcaniclastics. Beneath this section are hard, brown, non-laminated silty clays with vertical lines that may indicate pedogenesis. At ~7.21 m, the unlaminated brown silty clays transition into softer, speckled, green clays where a wavy contact appears to be the result of mixing during coring. We indicate a hiatus from 7.72–8.00 m due to known core loss, although it is unknown how much. Below this gap, sediments are mostly unlaminated, soft, sticky, brown clayey silts, with finer silty clays from ~9.33–9.6 m. Degradation of the metal lining of the core has resulted in sediment oxidation after ~9.6 m. At 11.14 m, the brown clays become soft and green with infilled burrows at the top of the section. From 11.54 m to the bottom of the core, sediments are volcaniclastic. At 11.72 m, 22 cm (11.72–11.94 m) were bulk dated to 38.9 ± 1.9 ka (Table 1). The similar age to the Menengai Tuff (35.62 ± 0.26 ka), which originated 12 km north of the coring site (Blegen et al., 2016), indicates these deposits likely represent a similar period of volcanic activity.

Uncertainties in correlation occur in several parts of the composite core, NAK. The unlaminated pedogenic muds from the top of the cores have few clear sedimentological features and low MagSus, causing complications in correlating NAK-X1 and NAK-Y1. The relationship between the cores is clearer between 1.54 and 6.07 m. NAK-X5I and NAK-Y5I&II were correlated using MagSus and μ-XRF data, but the correlation between NAK-X5II and NAK-Y5II is unclear. Due to limited sedimentological features, no MagSus data, and post-collection degradation of metal liners, correlation below this point was not possible. NAK-Y consists of several meters of tuffs below NAK-Y7II which are not visible in the NAK-X until NAK-X9I. There are two hypotheses for why this may have occurred: (1) Below ~7 m NAK-X shifted and was not cored completely vertically given the additional 1.5 m of brown clay before the Menengai Tuff. (2) The speckled green clays below 7.21 m may have infilled the hole during coring of NAK-X, evidenced by at least 70 cm of mixed sediment in X6I. Regardless of the reason, due to these correlation concerns, only NAK-Y samples were used for this study below 8 m.

4.2. Age model

A total of eight radiocarbon (out of 11 sampled) and two ⁴⁰Ar/³⁹Ar ages were successful, although one tephra (Ar01 at 6.01 m) resulted in an age reversal. The modern surface, eight radiocarbon dates, the Menengai Tuff, and the in-situ ⁴⁰Ar/³⁹Ar date were used for the age model (Fig. 3; Table 1). Initial runs of the age model indicated that the first two carbon dates do not fit well with standard accumulation rates. It is believed that the first age (NAK-AJ-17; located at 0.75 m, 0.93 ± 40 ka) was likely moved through bioturbation (Table 1). The second age (NAK-AJ-02; located at 1.25 m, 6.2 ± 60 ka) is near the end of the AHP but indicates an unrealistically slow accumulation rate. While, in general, the Naivasha and Nakuru-Elmenteita basins have low accumulation over the AHP due to basin filling (Bergner et al., 2009), it is still believed that there is a hiatus or erosional event where several to tens of cm of sediment, representing several hundreds to thousands of years, were lost. It is unclear what may have caused this, but the drill site is located just above a normal fault and at the slopes of Sirikon hill, which is >150 m high (Fig. 1C and D). A potential faulting event could have caused a

² Historically, *T. faurii* and *T. rudolfi* were indicated as having the same salinity preferences (Gasse et al., 1995), but further studies show that past analyses of *T. faurii* overstated its salinity preference (Roubeix et al., 2014). In addition, workers recognize *T. faurii* and *T. rudolfi* may represent a species complex (Hasle, 1978; Brindle et al., 2018), indicating that this ratio between deeper water, lower salinity preference *T. faurii* and shallower water, higher salinity preference *T. rudolfi* should indicate depth and/or dilution.

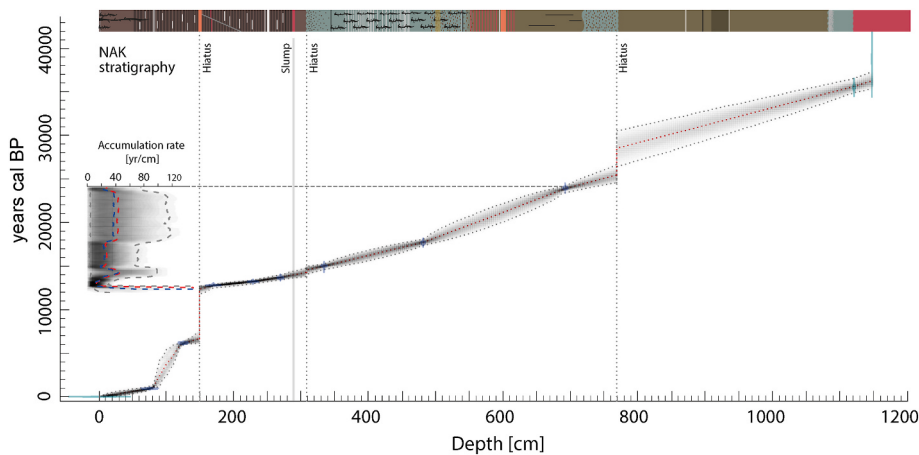


Fig. 3. Complete age model for NAK with stratigraphy and the accumulation rate for the part of the age model used for this study from 150 to 772 cm. A ghost plot shows the average (blue), median (red), and 95% confidence intervals (gray dotted lines). A slump occurs from 288 to 291 cm. Hiatuses occur at 149, 309, and 772 cm. (For interpretation of the references to color in this figure legend, the reader is referred to the Web version of this article.)

mass movement which led to the removal of such an amount of sediment. This hypothesis is supported by a small fault below starting just below the sand layer at 1.5 m.

In addition, the presence of a potentially large hiatus at 7.72 m isolates the sediments from the hiatus to the volcanics at 11.54 m. Because of this, there is low certainty in the lower part of the age model. The age model presented therefore only includes 1.5–7.72 m where there are multiple ages and only a short-term hiatus (~300 years) (Fig. 3, Suppl. 11). The accumulation rate is the slowest from 24–18 ka at ~38–40 yr/cm. From ~18–15 ka, the accumulation rate speeds up to ~20–22 yr/cm. The fastest rates occur after this point between ~14 and 12.6 ka with rates of ~12 yr/cm.

4.3. Core measurements

4.3.1. TC, TN, TOC, TOC/TN, WC

TC, TOC, and TN are highest in the upper 3 m of NAK (Fig. 4A, Suppl. 6). The ranges and averages of the top 3 m for TC are 0.3–5.6% and 3.7%; TN, 0.0–0.3% and 0.2%; and TOC, 0.2–5.2% and 2.8%, respectively. For the rest of the core, they are 0.1–1.7% and 0.4% for TC; 0.0–0.2% and 0.1% for TN; and 0.1–1.1% and 0.4% for TOC with only another increase at ~11.14 m within the soft, green clays with nodules. TOC/TN across the core ranges between 3.36 and 21.4 with an average of 11.2. Water Content mirrors lithology, with reduced water corresponding with larger grain sizes.

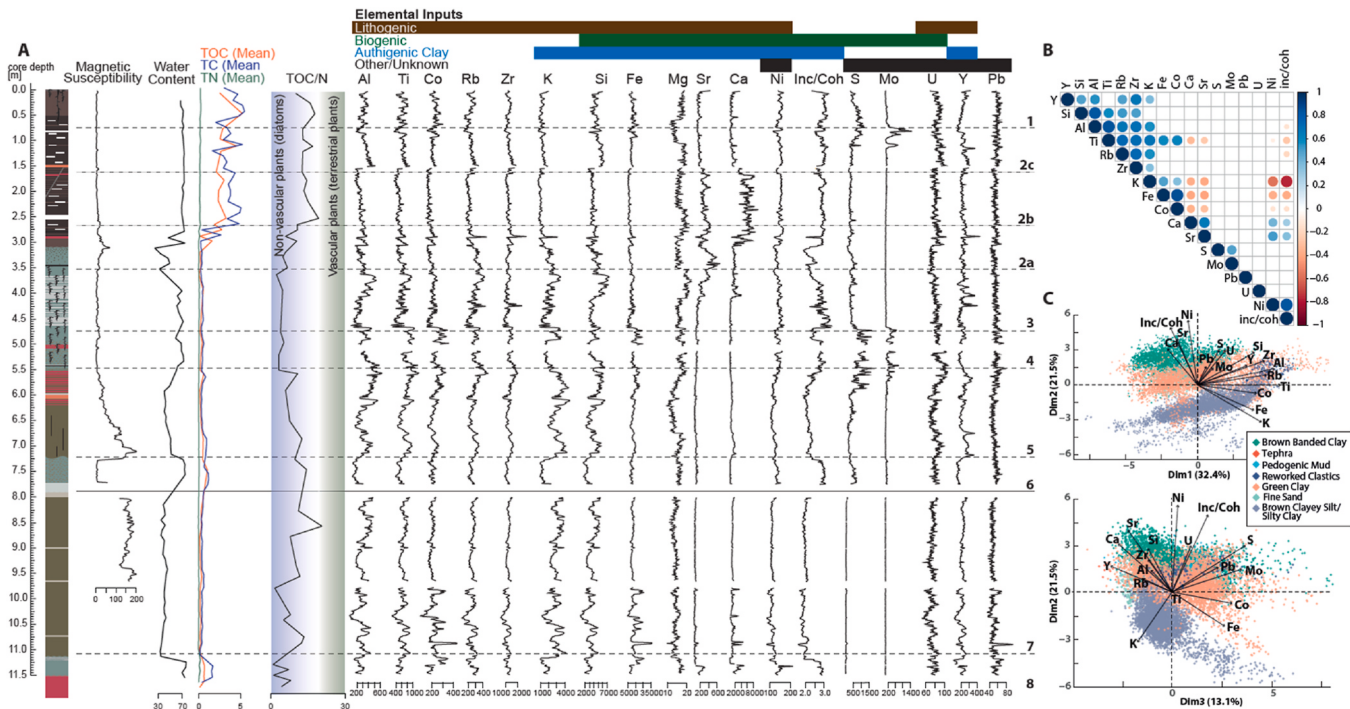


Fig. 4. A) NAK with smoothed magnetic susceptibility, TOC/N, TOC, TN, Water Content, and μ -XRF data in counts per second (cps) with the presumed source of the μ -XRF element highlighted above. TOC/N is highlighted so that the blue color represents periods of mostly phytoplankton input, whereas green indicates mostly terrestrial input based on Meyers (1994). Water content is measured in percent. All elements run in the PCA plus Mg B) Correlation Matrix of the different elements included in the PCA colored by significant positive or negative correlation. C) Biplots of μ -XRF PCA colored by the observed lithologies. Plots show Dim1/Dim2 and Dim2/Dim3, respectively. (For interpretation of the references to color in this figure legend, the reader is referred to the Web version of this article.)

4.3.2. Smoothed magnetic susceptibility and μ -XRF results

MagSus stays low for the upper ~5.6 m of the composite (range: 0.4–800; median: 87), with a deviation between ~2.8 and 3.35 m (Fig. 4A; Suppl. 2). MagSus begins to steadily increase at ~5.6 m with the transition into ash/green-brown clay layers. MagSus increases further leading into the hard, silty greenish brown clay where MagSus reaches 2100. There is then a drastic drop in MagSus after ~7.25 m at the soft green clays (19–200; 56). After the large hiatus between 7.72 and 8 m, MagSus is high (1000–2100; 1600) for the unlaminated brown clays.

All elements with a positive median (Suppl. 5) are featured in Fig. 4, but only those used in the PCA, as listed in section 3.3.2., are discussed further. Lithogenic elements include Al (range: 63–720 cps; median: 300 cps), Ti (150–1300; 630 cps), Co (34–480; 210 cps), Rb (81–500; 260 cps), Zr (380–3400; 1300 cps), U (39–160; 80 cps), and Y (74–600; 230 cps). Elements that are lithogenic but also impacted by authigenic biological and clay components include K (520–5100; 2100 cps), Si (880–7700; 3800 cps), and Fe (3150–40,100; 10,900 cps). The Sr (20–720; 110 cps) and Ca (110–13,000; 1000 cps) records have alloogenetic components, but also appear to be impacted by authigenic components, with the largest increases above ~4.1 m. Nickel (72–240; 130 cps) varies subtly but appears to increase around the green clays. Similarly, incoherence/coherence (inc/coh) (1.5–1.6; 2.5), which is often used as an indicator of organic matter content (Burnett et al., 2011; Davies et al., 2015; Giralt et al., 2011) but can also indicate changes in clay or water content, increases in the green clays, but also in the top ~3.10 m of the core, indicating its authigenic controls. Sulfur (0–2700; 330 cps) and Mo (0–1, 710; 65 cps) show a similar flat trend across the core except around areas with thick white laminations above ~1.15 m and between ~4.6 and 6.0 m and often are controlled by biological factors. Lead (9–130; 53 cps) varies across the core with no clear trend, making its origins less clear.

4.3.3. PCA

Only the first three dimensions of the PCA were explored, as together they represent 67% of variation with other individual components representing <6% of the variance (Suppl. 4). Dimension 1 (Dim1) represents 32.4% of the data with Ti, Al, Rb, Zr, K, Co, Si, Fe, and Y exerting significant, positive control (Fig. 4C). We observe that reworked clastic samples plot positively along Dim1 and more laminated sediments such as the brown banded clays plot more negatively. We therefore interpret Dim1 to represent a positive alloegenic input from less weathered igneous sources and a negative authigenic clay deposition. Consequently, an increase in Dim1 can be interpreted as an increase in precipitation which enhances surficial erosion and lithogenic flux. Dim1 is highly variable and generally greater than 0 at ~10.5–11.2 m, ~9.4–10.2 m, ~8.0–8.8 m, ~4.7–7.25 m, ~3.35–4.4 and above ~1.5 m (Fig. 5). Dimension 2 (Dim2) represents 21.5% of the data with Ni, inc/coh, Sr, Ca, S, U, and Si controlling it positively and only K significantly controlling it negatively. The observed lithologies of the composite core are well organized, with brown banded clay plotting the most positively, unlaminated brown clays plotting the most negatively (Fig. 4C). Pedogenic muds, green clays, sands, tephras, and reworked clastics all plot slightly positive but closer to zero. Because Ca and Si are the major elements governing the process/source of Dim2, and by considering the geochemical behavior of other (trace) elements, it is very likely that both organic matter- and secondary deposition Ca-Na bearing precipitates control this group. This suggests that carbonates (biological and/or lithological) could have been deposited during wetter phases at Nakuru. A biologically-linked process is possible due to an increase in nutrient supply to the lake during wetter periods and consequent increase in bio-productivity. At the same time, enhanced bio-productivity can indirectly catalyze carbonate production (and precipitation) through water pH increase in response to CO₂ consumption. The interpretation of K, the lone significant negative element in Dim2 is less straightforward as it can also

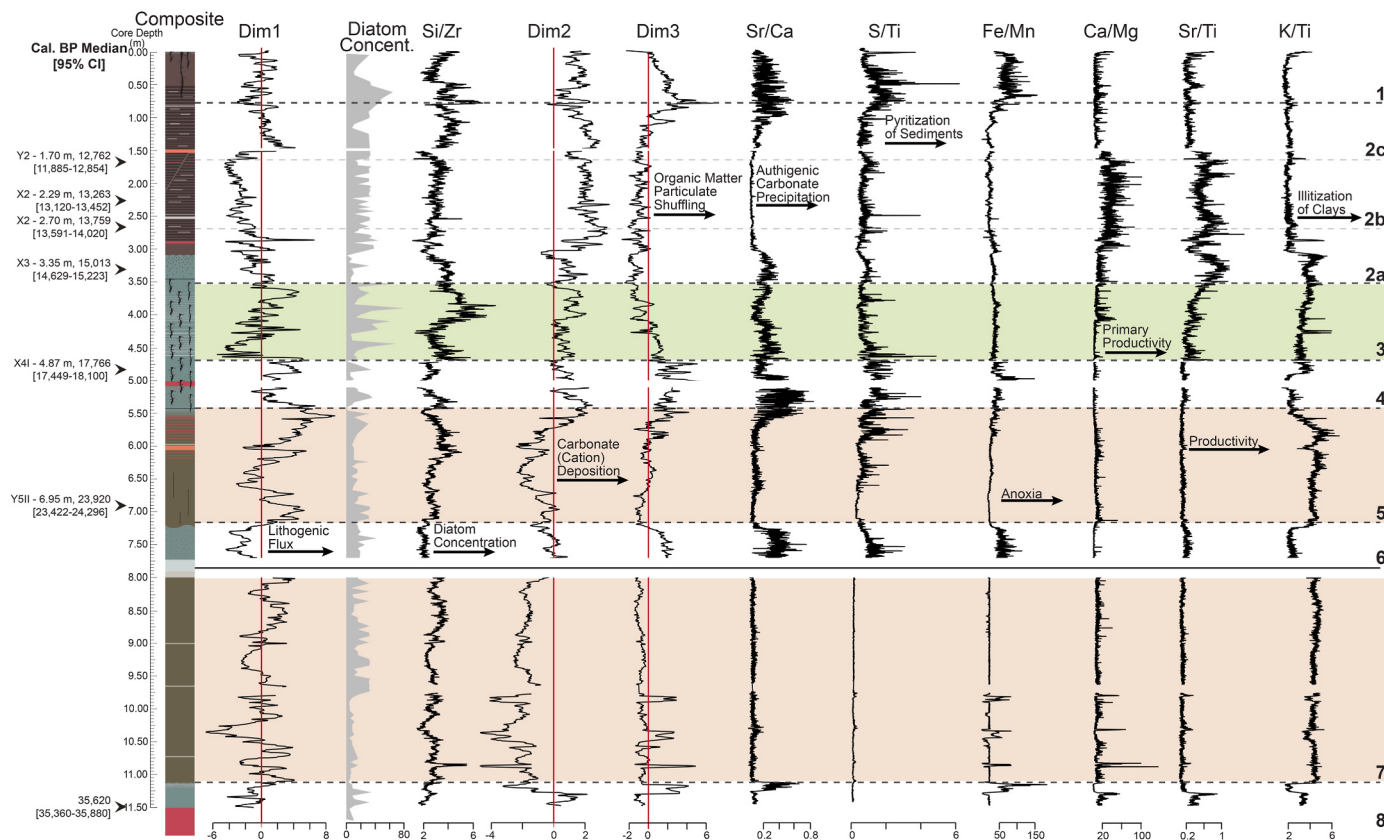


Fig. 5. NAK with ages alongside the smoothed PCA loadings of Dim 1, 2, and 3; diatom concentration, and important μ -XRF ratios, including Si/Zr, Sr/Ca, S/Ti, Fe/Mn, Ca/Mg, Sr/Ti, and K/Ti. The interpretations for these variables are included in the figure and further extrapolated upon in section 4.3.

deposit authigenically under drier conditions (Foerster et al., 2018), and in this case, we also cannot fully deconvolute the contribution from the reworked clastics and authigenic contributions. Dim2 fluctuates slightly throughout NAK but is almost consistently above 0 below ~11.3 m and above ~5.8 m (Fig. 5). Dimension 3 (Dim3; 13.1% of variance) is controlled by S, Mo, Co, Fe, and Pb positively and Y, Ca, and Sr negatively. This dimension is most pronounced between 7.25 and 8 m, 4.75–5.5 m, and above 1 m (Fig. 5) (enrichments along the metal liners excluded). In the absence of anthropogenic influence and/or punctuated volcanic events associated with the respective depths of enrichment, these elements are indicative of organic matter particulate shuffling, including that of plant debris and phytoplankton. The presence of Mo, which is key in nitrogen fixation, and S and Fe, which can be oxidized by microorganisms, indicate that Dim3 likely highlights phases of anoxia which appear to be negatively correlated with carbonate deposition phases.

The correlation matrix (Fig. 4B) shows how strongly correlated the lithogenic elements (Y, Si, Al, Ti, Rb, Zr, K, Fe, and Co) are. Some of these elements, Ti, Fe, Rb, Co, and especially K, negatively correlate with biogenic cations, like Ca and Sr, and clay indicators, like inc/coh and Ni. This indicates that element deposition is governed by two main sediment types: those less-weathered and those controlled by cation deposition through biological and/or lithological authigenic processes. This indicates a negatively-correlated relationship between weathering (likely related to rainfall) and biological/Ca-Na bearing salt deposition during drier periods of decreased weathering.

4.3.4. μ -XRF ratios

The ratios selected for further investigation include Si/Zr, Sr/Ca, S/Ti, Fe/Mn, Sr/Ti, and K/Ti (Fig. 5). Despite the low Mg intensity detected (range: 2.9–31.2 cps) and thus higher uncertainty of the enrichment excursions, we include Ca/Mg because it has been shown to be a good proxy for primary productivity and highlights the biological components of Dim2. Although Si is partly controlled by Dim1, Si/Zr,

which mirrors diatom concentration, is highly variable, indicating that diatom productivity (Burnett et al., 2011) may have been higher in the top ~6.2 m compared to the bottom of the core. Sr/Ca, S/Ti, and Fe/Mn all show similar trends to Dim3 (increases from 7.25–8, 3.1–5.75, and above 1.15 m), indicating phases of anoxia as well as a negative correlation between Ca and anoxic conditions. Ca/Mg and Sr/Ti are highest in the top ~4.1 m of the core, with the largest peaks from ~1.45–3 m, indicating increases in primary productivity (Naehler et al., 2013; Davies et al., 2015). Lastly, Ti/K, which indicates increased illitization of clays and likely decreased precipitation (Foerster et al., 2018), peaks below 8.0, ~5.55–7.25, and ~3.05–4.95 m except for a decrease between ~11.10 and 11.25 m.

4.4. Diatom results

Observed diatoms often increase in abundance with other diatoms historically documented together in a certain habitat (Fig. 6; Suppl. 8, 10). Benthic taxa including *Encyonema muelleri* (Hustedt) Mann, *Epi-themis adnata* (Kützing) Brébisson, *E. gibberula* (Ehrenberg) Kützing, *Nitzschia fonticola* (Grunow) Grunow, *N. palea* (Kützing) Smith, *N. palea* var. *debilis* (Kützing) Grunow, *Pantocsekia ocellata* (Pantocsek) Kiss & Ács, and *Pseudostaurosira brevistriata* (Grunow) Williams & Round are most abundant between ~11.15–8.0, ~7.25–5.5, and ~2.7–1 m. Other taxa such as *Aulacoseira granulata* (Ehrenberg) Simonsen, which is planktonic, and the low-silicified centric species (*Thassiosirales* sp. 2 Glezer & Makarova), whose taxonomic designation is unknown, also follow the patterns of the benthic taxa. Both *Thalassiosira faurii* (Gasse) Hasle and *Thalassiosira rudolfi* (Bachmann) Hasle, as planktonic taxa, occur concurrently and are most abundant from ~7.72–7.25, ~5.45–4.7, and ~3.55–0.8 m, with *T. rudolfi* also abundant below 11.15 m. The largest deviation along the core occurs between ~4.6 and 3.55 m where *Stephanocyclus meneghinianus* (Kützing) Skabichevskij, a littoral, planktonic species, becomes incredibly abundant. Eight zones based on the total diatom assemblage were created using Bray-Curtis dissimilarity

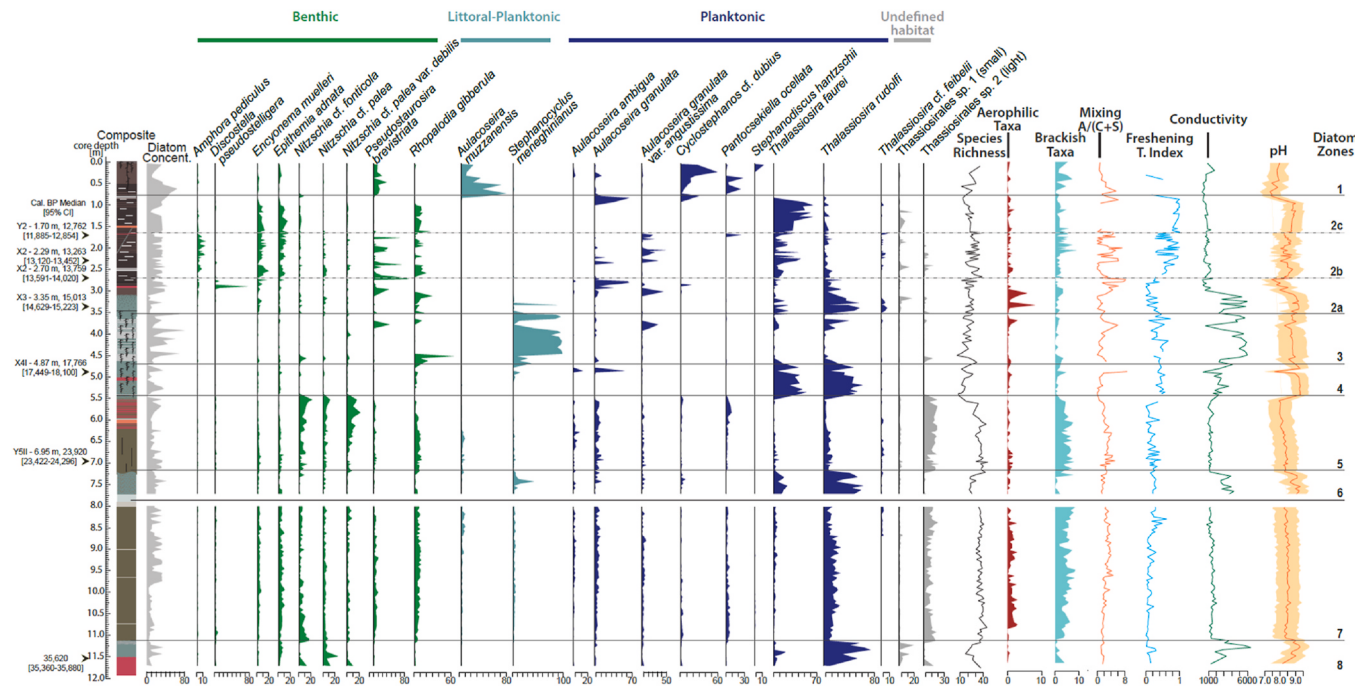


Fig. 6. Diatom concentration calculated as described in methods. The diatom taxa that reached $\geq 10\%$ in at least one sample are then included and organized by habitat with green as littoral (shoreline), light blue as littoral planktonic, and dark blue as planktonic. Diatoms with unknown habitats are in gray. Species richness is also included. The diatom proxies include the conductivity and pH results from the transfer function by Gasse et al. (1995), a mixing proxy (A/(C + S)) based on Gasse et al. (2002); a fresh, deep water proxy (*T. faurii*/*T. faurii* + *T. rudolfi*) from this study; and aerophilic and brackish taxa based on Gasse (1986) and Taylor et al. (2007) included in Supplemental 10. The various zones are included created using hierarchical clustering with Bray-Curtis dissimilarity with all of the diatom counts. (For interpretation of the references to color in this figure legend, the reader is referred to the Web version of this article.)

and mostly follow lithological changes in the core. The boundaries occur at 0.8, 3.55, 4.75, 5.45, 7.25, 8 (the large hiatus), and 11.14 m.

Diatom concentration is variable across the core, with the highest peaks in the white sections of the green laminated clays (Fig. 6). Species richness inversely follows changes in *Thalassiosira rudolfi*, where between 11.5–11.2, 7.80–7.20, and 5.4–4.7 m *T. rudolfi* increases while species richness decreases. The calculated conductivity (range: 193–6380 $\mu\text{S}/\text{cm}$) is nearly always above 1000 $\mu\text{S}/\text{cm}$ with peaks $>3000 \mu\text{S}/\text{cm}$ between ~11.5–11.2, ~7.72–7.25, and ~5.5–3.05 m (Suppl. 9). The pH (range: 7.3–9.4) follows a similar trend, but with a longer alkaline phase between ~5.45 and 0.9 m. The mixing proxy, A/(C + S), is the lowest within the green clays and has the largest spikes above ~3 m. The T. Index, which indicates freshening conditions, gradually increases over time with two jumps at ~5.45 and ~2.75 m. The abundance of aerophilic taxa is low with increases at ~3.75–2.95 m and ~10.8–8 m. The abundance of brackish taxa tends to increase in zones with an increase in benthic taxa, especially between ~7.3–5.5 and ~11.1–8 m.

5. Discussion

5.1. Lake Nakuru's unique proxies

The deposition, chemistry, and productivity of lakes are determined by their vertical and horizontal morphology, altitude, energy input/output, physical input/output, local climate, long-term climate, and biotic influences (Talling, 2001). To best understand environmental change through lake sediments, we must understand how these variables relate to one another and impact different proxies. Often, shallow, tropical lakes like Nakuru have chemical responses that are “ecologically dominant,” meaning that lake biota greatly impact its geochemical signature and deposition (Talling, 2001). Lake Nakuru's high primary productivity, as well as other unique variables such as its closed basin, highly alkaline source rocks, amplified response to climate change, high elevation, and minimal riverine input (Fazi et al., 2018), control its sedimentological, biological, and chemical changes, highlighting the necessity of careful examination using multiple high-resolution proxies.

5.1.1. Anoxic/oxic deposition at Paleolake Nakuru

The sedimentological facies deposited at NAK indicate distinct phases of anoxic and oxic depositional conditions. The green clays within the core indicate deposition during anoxia (IUSS Working Group, 2014), appearance of pyrite (Junginger, 2006), and increase in Fe/Mn (Fig. 5). Anoxic conditions in lakes can be caused by exceedingly high biological productivity due to an increase in nutrients (Lung'aya et al., 2001; Ndebele-Murisa et al., 2010; Brothers et al., 2014); deep water that creates anoxic bottom waters (Pilskaln and Johnson, 1991; Owen and Crossley, 1992; Hecky et al., 1994); a decrease in mixing such as through decreased wind or a change in wind direction (MacIntyre et al., 2012); or a decrease in temperature/density gradients (De Cort et al., 2013; Kragh et al., 2020). Within the green clays, lithogenic elements (Fig. 4) and Dim1 (Fig. 5) decrease, indicating limited clastic deposition. In contrast, inc/coh (Fig. 4) and Dim2 (Fig. 5) increase, indicating more organic matter (Burnett et al., 2011; Davies et al., 2015), potentially related to increased productivity or preservation (Mahamat Ahmat et al., 2017). Within the diatomaceous laminated green clays, inc/coh, Mo, and S are elevated (Fig. 4). With an extrapolated accumulation rate of ~13 yr/cm (Fig. 3), this may relate to seasonal mixing and temporary anoxic conditions such as that observed at other lakes in eastern Africa (Pilskaln and Johnson, 1991; Owen and Crossley, 1992) and typical in eutrophic soft water lakes with seasonal algal communities (Brauer, 2004). The cause of lamination is unknown and dependent on the lake itself given that tropical lakes can produce laminated clays due to (a) increased mixing during the dry season due to increased wind strength (Hare and Carter, 1984), (b) increased mixing during the wet season due to increased external hydrological input (Egborge, 1979), (c) permanent deep water anoxia resulting in dark layers from sediment input in the

rainy season and light layers from diatom input during the dry, windy season (Pilskaln, 2004), or (d) a completely alternative mechanism that results in fine-grained laminations.

Across the rest of the core, sediments were oxygenated. The brown clays are interpreted as shallower, oxygenated layers, based on high lithogenic/igneous components with low biogenic components (Fig. 4) and vertical dark lines indicating pedogenesis between ~6.05 and 7.25 m, although there is currently no evidence for an extended hiatus during this phase (Fig. 2). The graded increase in sands from ~3.44–3.09 indicates a gradual increase in high-energy deposition such as from an alluvial fan, river, or shoreline. These sands, dated to ~15 ka (Table 1), are interpreted as the beginning of the AHP, where an increase in rainfall could lead to an increase in high energy deposition. At ~3.09 m, a sharp transition from sands to muds indicates a potential hiatus. After 15 ka between 3.09 and 1.5 m, the slight decrease and reduced variability of lithogenic/igneous elements (Fig. 4) and Dim1 (Fig. 5) indicate an increase in chemical over physical element deposition. The laminated brown muds above this section indicate oxygenated sediments undergoing cyclic rainfall and/or changes in paleoproductivity. In addition, above 3.09 m, inc/coh, Ca, Sr, TOC/N, TOC, and TN all increase (Fig. 4), indicating increased primary productivity and/or preservation. The reworked volcaniclastics at 1.49–1.54 m deposited after 12.8 ka indicate the potential for high-energy events to bring larger clasts into the system, similar to the sands between ~3.09 and 3.44 m, potentially after a lake level drop. With a 6.2 ka charcoal at 1.25 m, a large hiatus is evident and complicates the reliability of the age model above this point. Most sediments from the AHP are missing from the NAK core – an observation also visible in the Richardson and Dussinger (1986) core (Fig. 2). We hypothesize that the coring site is located close to a fault, which is indicated by the steep slope adjacent to the coring site (Fig. 1D). It is believed that a mass-wasting event due to localized faulting occurred after 12.8 and before 6.2 ka (explained in section 4.2), removing a substantial portion of the AHP sediments. The sediments located above 1.25 m have been reworked by roots and represent slower deposition.

5.1.2. Evaluation of *Thalassiosira rudolfi* as Paleodepth indicator for Lake Nakuru

Diatoms and other micropaleontological proxies like ostracods are used as conductivity and pH indicators within closed basins to represent changing depths (e.g., Cohen et al., 1983; Richardson and Dussinger, 1986; Gasse et al., 1995; Barker et al., 2002; Birks et al., 2010), yet the evidence of anoxic phases from this study indicate that this interpretation may not be valid for NAK. *Thalassiosira rudolfi* is a well-documented high alkalinity preference diatom taxon whose increase in closed basins has been used to indicate shallowing conditions (e.g., Halfman et al., 1992; Gasse et al., 1995; Owen et al., 2014; Muiruri et al., 2021). Within the NAK core, however, *T. rudolfi*-rich, anoxic green sediments (>11.14, 8–7.25; and 5.45–4.75 m) are unlikely to represent shallowing conditions (Fig. 6). While shallow lakes can be anoxic, it is uncommon for these conditions to last more than several days to months (Brothers et al., 2014; Kragh et al., 2020). Increased *T. rudolfi* phases are also accompanied by decreased species richness. Other high alkalinity indicator taxa, like *Stephanocyclus meneghinianus*, *Anomoeoneis sphaerophora* Pfitzer, *Mastogloia elliptica* (Agardh) Cleve, and *Nitzschia frustulum* (Kützing) Grunow, and shallow water taxa, like *Epithemia adnata* and *E. gibberula*, are relatively absent from these zones (Fig. 6). Instead, the well-oxygenated brown clays with evidence of pedogenesis have increased species richness and littoral and brackish taxa, indicating shallower conditions in these zones. Geochemical proxies, including a decrease in lithogenic/igneous elements (Fig. 4) and K/Ti (Fig. 5), also indicate that *T. rudolfi* phases are likely not shallowing. Instead, we propose five hypotheses of what might cause the variation between the low-diversity, *T. rudolfi*- and the high diversity, benthic-layers below 4.75 m: (Hyp1) groundwater flow, (Hyp2) mixing, (Hyp3) depth, (Hyp4) nutrient loading, or (Hyp5) closedness of the lake system.

(Hyp1) Changes in groundwater could come from increased

hydrothermal activity or groundwater connections between Naivasha and Nakuru-Elmenteita (Dühnforth et al., 2006; Olaka et al., 2010) controlled by climatic, volcanic, or tectonic variables. These changes could impact the hydrochemistry, mixing, nutrient loading, and/or depth of Lake Nakuru. (**Hyp2**) Changes in mixing could occur due to changes in wind strength, depth, temperature, and/or seasonality. Given limited evidence of large tectonic processes changing basin shape over the last 36 kyr (McCall, 1967), these variables are likely controlled by climate. (**Hyp3**) Changes in depth are controlled by rainfall, either through direct precipitation/surface flow or groundwater flow. (**Hyp4**) Changes in nutrient loading at Lake Nakuru would likely come from increased rainfall, due to the already high concentrations of Si in Lake Nakuru which would limit volcanic activity such as hydrothermal or volcanic ash input's impact on nutrient loading. (**Hyp5**) Changes in whether Lake Nakuru is an open or closed basin relate to Nakuru's connection with Elmenteita or Menengai which have been hypothesized, and proven in the case of Elmenteita, by previous workers (Washbourn-Kamau, 1971; Cohen and Nielsen, 1986; Richardson and Dussinger, 1986; Dühnforth et al., 2006). Such changes between Lake Magadi and Natron have been observed to impact the diatom record (Gasse et al., 1997). A connection between Lake Nakuru with Elmenteita would only occur if Nakuru was ~80 m deep and with Menengai if Nakuru was ~186 m deep, supporting Hyp3.

It is currently unclear which of the hypotheses created the anoxic conditions and increased *T. rudolfi* visible in NAK. Changes in groundwater (Hyp1) cannot currently be constrained with our proxies but would influence other variables (Hyp2-4). The decreased diversity within the *T. rudolfi* horizons might indicate reduced mixing (Hyp2) and/or increased depth (Hyp3), as diversity tends to increase closer to shore with heavier mixing (e.g., Stevenson and Stoermer, 1981; Moos et al., 2005; Cantonati et al., 2009; Laird et al., 2010; Hayashi, 2011; Laird et al., 2011). Decreased mixing (Hyp2) is supported by A/(C + S) which decreases within the *T. rudolfi*-rich sections (Fig. 6). The high diversity sections below ~4.75 m also have increased benthic and brackish taxa, indicating that these phases may have been better mixed (Hyp2), more alkaline, and/or shallower (Hyp3). Potential deepening (Hyp3) of the *T. rudolfi* horizons is supported by a decrease in K/Ti (Fig. 5) and inc/coh (Fig. 4) since tropical lakes often increase in primary productivity during the wet seasons (Zébazé Togouet et al., 2007). It is therefore difficult given our proxy records to separate increased mixing (Hyp2) and deepening (Hyp3). If the *T. rudolfi* horizons are controlled by nutrient loading (Hyp4), those controls are likely climatic. Increased precipitation could result in increased nutrients and algal blooms due to increased chemical weathering and erosion of volcanic source rock into Lake Nakuru. Alternatively, in drier/evaporative conditions, nutrient loading could increase from increased evaporative nutrient concentration, reworking of sediments, or oxidation of sediments that could release P into the lake. Despite evidence of high volcanic activity resulting in algal blooms in both modern and ancient contexts (e.g., Kurenkov, 1966; Yuretich, 1982; Thevenon et al., 2002; Duggen et al., 2010; Yuan et al., 2019), increased volcanic activity does not seem feasible as a mechanism for increased nutrient loading at Nakuru, whose lithic input already comes from volcanic source material. Given the impact of many of these hypotheses on one another, it is anticipated that the increased *T. rudolfi* results from the combination of these variables, but likely in relation to some increase in depth/precipitation given that increased precipitation can result in decreased mixing (Hyp2), deepening (Hyp3), and increased chemical weathering (Hyp4).

5.2. 35 kyr of hydroclimate change at Lake Nakuru and across the EARS

Nakuru was always at least slightly alkaline (pH >8) based on the diatom transfer function (Fig. 6), even during deeper conditions. General trends throughout the core indicate freshening, deepening (T. Index; Fig. 6), and an increase in carbon deposition (Dim2; Fig. 5) with eight

diatom zones highlighting different hydrological phases. The most robust portion of our age model documents changes from Zone 6 (~25 ka) to the middle of Zone 2b (~12 ka) (Fig. 3), with the other zones (8, 7, 2c, and 1) revealing important hydrological changes, including seemingly cyclic anoxic/oxic phases, but without strong age constraints.

5.2.1. Zone 8 – anoxic, productive lake – ~35.6 ka to unknown, 11.5–11.14 m

Zone 8 (~35.6 ka-Unknown, 11.5–11.14 m) represents deposition of the Menengai Tuff followed by an anoxic, low-diversity, *Thalassiosira rudolfi* phase, indicating deeper waters and/or increased stratification. This zone indicates high levels of productivity with an increase in Dim2, Ca/Mg, Sr/Ti (Fig. 5), and TN (Fig. 4) likely due to enhanced detrital input from the catchment as indicated by negative Dim1 (Fig. 5). Refilled burrows at the top of this zone reflect this zone's high productivity but ultimate shallowing and desiccation leading to Zone 7 (Fig. 2).

Other areas across the EARS indicate short-term wet pulses between ~38 and 33 ka. The well-dated Chew Bahir K-record exhibits a wet phase from ~37–35 ka, with the last wetness pulse ~35 ka (Foerster et al., 2012) (Fig. 7). This is also highlighted by high lake levels at Lake Tana reflected by the Ca/Ti record (Lamb et al., 2018). Nile discharge is enhanced from 37–35 ka, indicating higher precipitation on its eastern African tributaries (Ehrmann et al., 2016). At Lake Tanganyika, in the western branch, at ~37 ka there is an ~6 kyr increase in precipitation evident in the δD record (Tierney et al., 2008), which is also evident in other Tanganyika records including Burnett et al.'s (2011) biogenic silica and Rb/K which indicate a change in source, potentially related to an increase in precipitation. The record from the Burundi Highlands also indicates increased precipitation with two peaks in the nonsmoothed data at ~35 and ~34 ka (Bonnefille and Chalié, 2000). At Lake Masoko, the record instead shows dry conditions with wetter conditions before 35 ka (Barker et al., 2003).

5.2.2. Zone 7 – shallow, oxygenated lake/land surface – unknown, 11.14–8 m

Zone 7 (11.14–8 m) is interpreted as a well-mixed zone with phases of desiccation due to its brown clayey-silty sands with organic-rich dark, fine layers. TOC/N from 4–10 indicates mostly algal input whereas TOC/N >20, mostly vascular land plant input (Meyers, 1994, 2003). Zone 7 (TOC/N range 4–21.4) therefore seems to indicate the mixed algal-/vascular land plant input (Fig. 4) of a dynamic flood plain with little organic material (Dim2, Fig. 5). The elevated insoluble lithogenic and igneous elements (Fig. 4) and K/Ti (Fig. 5) support a less weathered regime with less rainfall as do increased aerophilic taxa which imply periods of aerial exposure (Fig. 6). Across Zone 7, the taxa indicate shallow waters with benthic taxa such as *Epithemia adnata*, *E. gibberula*, *Nitzschia fonticola*, and *Pseudostaurosira brevistriata*, ranging from 29–57% of the assemblages with a median of 44%. The only common planktonic diatom, *Thalassiosira rudolfi*, illustrates that the waters were slightly alkaline, with a calculated conductivity of 1400 μS/cm and a pH of 8.5.

While the age of NAK in this zone is unclear, it must be much older than ~25.5 ka. Very few eastern African lacustrine records exist earlier than 25 ka, likely a result of dry conditions across the region. Available records in Ethiopia show drying with only brief peaks in humidity from Chew Bahir post-35 ka (Foerster et al., 2012) and a pronounced drying of Lake Tana at ~31 ka (Lamb et al., 2018). Lake Tanganyika post-31 ka (Tierney et al., 2008) and the Burundi Highlands post-34 ka also exhibit drier conditions (Bonnefille and Chalié, 2000) (Fig. 7). Lake Masoko, a southern hemisphere record, indicates wetter conditions (Barker et al., 2003). The Nile discharge (Ehrmann et al., 2016) remains higher, most likely due to continued higher moisture availability in the western EARS.

5.2.3. Zone 6 – deeper, anoxic lake – ~25.5 to 24.5 ka, 8–7.25 m

Zone 6 (~25.5–24.5 ka, 8–7.25 m) returns to soft green clays

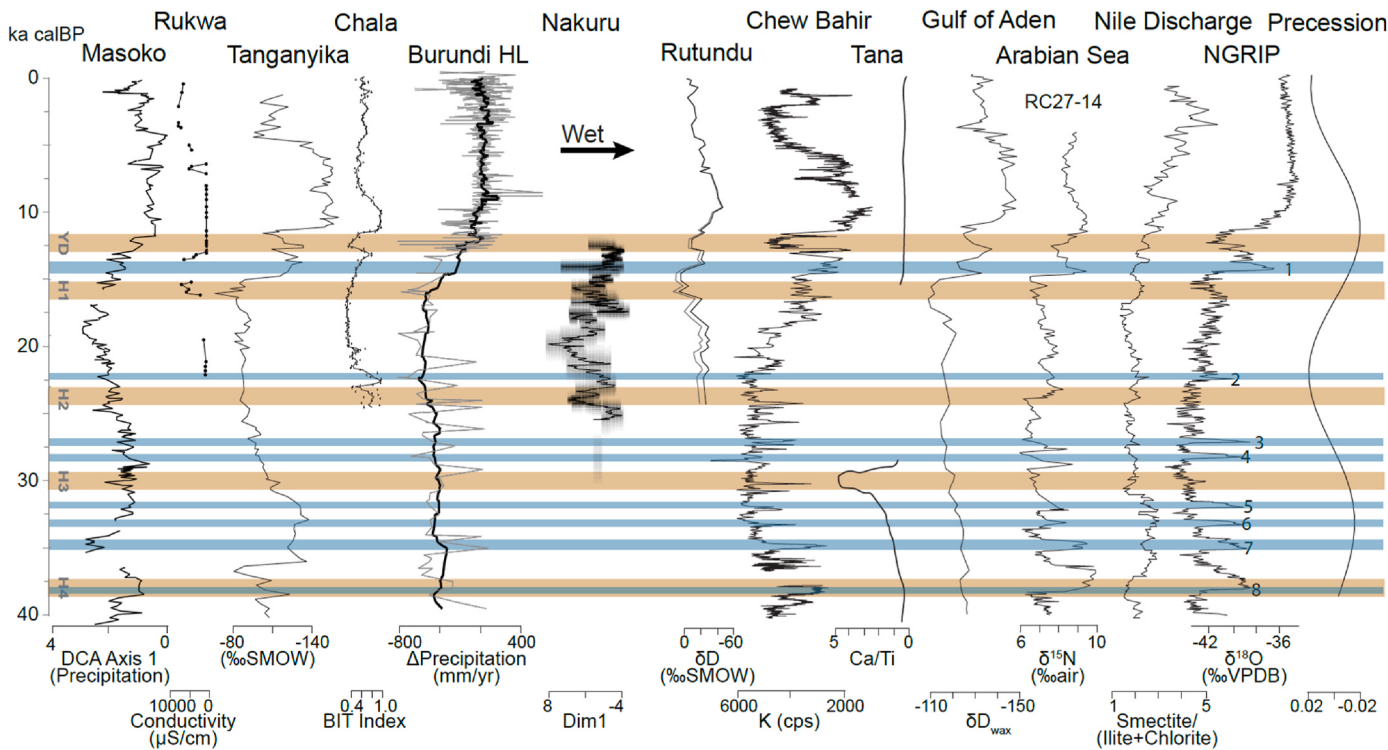


Fig. 7. Comparison of lake records from across the EARS with general wetter conditions (regardless of the exact proxy) plotting to the right adapted from Foerster et al. (2012). These are compared with the precession cycle (Bergner et al., 2009), Dansgaard-Oeschger (DO) events (blue), and Heinrich (H) events (tan). DO and H events are numbered and dated based on NGRIP δ¹⁸O (North Greenland Ice Core Project members, 2004). The Nile record from Ehrmann et al. (2016) is a clay record from GeoTü SI110 where increased smectite/illite + chlorite indicates increased sediment discharge. The Arabian Sea record from core RC27-14 is from Altabet et al. (2002) using δ¹⁵N as a proxy for denitrification and productivity in the Gulf of Oman. The Gulf of Aden record is from δD of leaf wax to record precipitation variability from Tierney and deMenocal (2013) with a reversed scale. The Lake Tana record with a reversed scale from Lamb et al. (2018) is of Ca/Ti, a proxy for effective moisture. Chew Bahir K record is from Foerster et al. (2012), with a reversed scale, as a wetness proxy. The reversed scale δD left wax record from Garelick et al. (2021) represents the proxy for Lake Rutundu on Mount Kenya. The dark line represents the leaf wax data corrected for vegetation and global ice volume whereas the lighter gray line is only corrected for vegetation. The Nakuru record (this study) uses a ghost plot and median of K/Ti and Dim1 with reversed scales as wetness proxies. The Burundi Highlands record is a precipitation change estimate in mm/yr from pollen records from Bonnefille and Chalié (2000) with the average in black. The Lake Chala record is a BIT Index which is interpreted as precipitation proxy from Verschuren et al. (2009). The Lake Tanganyika record is from δD of leaf wax to record precipitation variability from Tierney et al. (2008) with a reversed scale. The Lake Rukwa data from Barker et al. (2002) uses a diatom transfer function of conductivity for lake depth/moisture. The Lake Masoko record from Barker et al. (2003) uses DCA Axis 1, a precipitation-evaporation proxy for water depth based on diatom data. (For interpretation of the references to color in this figure legend, the reader is referred to the Web version of this article.)

dominated by *T. rudolfi*. While *T. rudolfi* is the dominant taxa, this phase includes more *T. faurii* compared to Zone 8 (Fig. 6), showing that conditions may have been slightly wetter. This phase indicates high productivity (inc/coh, Dim2), authigenic carbonate precipitation (Sr/Ca), and anoxia (Dim3, S/Ti, Fe/Mn) (Fig. 5; 9) that appear to be the result of wetter conditions, indicated by decreased Dim1 and K/Ti compared to Zone 7 (Fig. 5).

Earlier Lake Nakuru records may also show this wet phase with Cohen et al.'s (1983) ostracod transfer function reflecting deeper conditions >24 ka (Fig. 8) not observed in the diatom record (Richardson and Dussinger, 1986). Our results support not only deeper conditions around this time, but also that a diatom-based conductivity transfer function at Lake Nakuru may not be an accurate depth indicator as highlighted in 5.1.2.

In the eastern African records, multiple wet phases are visible around ~27 ka and ~25 ka despite general drier conditions, including at Chew Bahir (Foerster et al., 2012), Lake Tanganyika (Tierney et al., 2008), and Masoko (Bonnefille and Chalié, 2000) (Fig. 7).

5.2.4. Zone 5 – shallow lake/land surface with pedogenesis – 24.5 to 19.5 ka, 7.25–5.45 m

Zone 5's (24.5–19.5 ka, 7.25–5.45 m) dominant lithology consists of a dense and compact greenish-brown silty clay with intercalated silt beds and vertical lines indicating pedogenesis. From 6.2 m upwards,

sediments become sandier from numerous thin ash layers surrounding a reworked tephra at ~6 m dated to 36.5 ka (Fig. 2). Zone 5, which resembles Zone 7, reflects the dry conditions of the LGM with low organic matter (Dim2, inc/coh) and increased species richness with many benthic diatoms, *Thallasiosirales* sp. 2, and *Aulacoseira granulata* (Fig. 8). The shallow conditions are also reflected by low carbon precipitation (Sr/Ca), predominantly igneous input (Dim1), high illitization (K/Ti), and oxygenated water (low Fe/Mn, Dim3) (Fig. 5). At ~5.8 m (20.5 ka), the record at Nakuru indicates a gradual change towards wetter conditions over ~1 kyr with a color change from brown to green sediments (Fig. 8). In addition, there is evidence of deepening through an increase in inc/coh and decrease in K/Ti. After 22 ka, high alkalinity-preference taxa like *Epithemia gibberula* and *Thallasiosira rudolfi* decrease and freshwater, benthic taxa like *Nitzschia fonticola*, *N. palea* series, and *Pantosekiella oscellata* increase.

At most localities in eastern and northern Africa more broadly (e.g., Porter and Zhisheng, 1995; Gasse, 2000), the records are dry during the LGM 26.5–19 ka (Clark et al., 2009). While most records do not have high enough resolution to show the rate of change out of the AHP, Chew Bahir's record seem to match our record well (Foerster et al., 2012) (Fig. 7). Lake Rutundu at near-by Mt. Kenya (Garelick et al., 2021), records higher precipitation, as does Lake Chala on the eastern flank of Mt. Kilimanjaro (Verschuren et al., 2009) (Fig. 8).

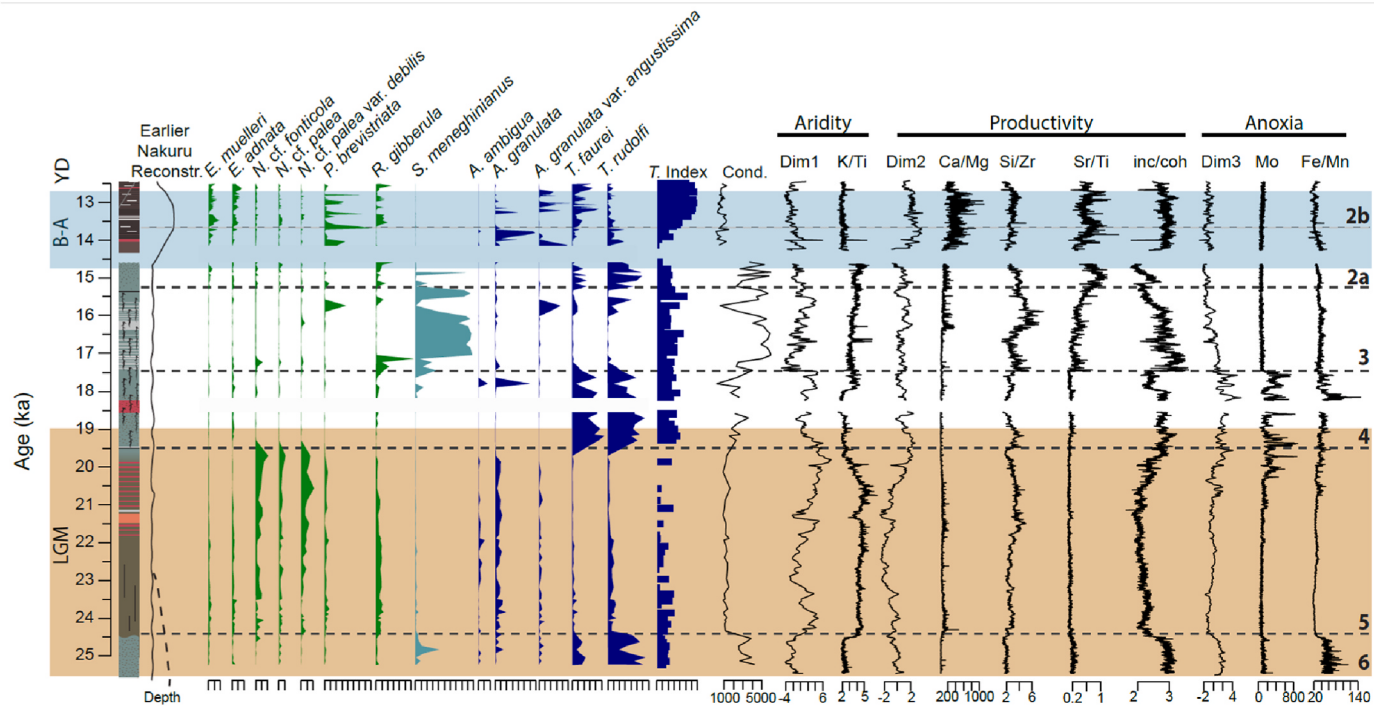


Fig. 8. Important parameters along the age model for NAK including diatom taxa that represent >10% in one sample with each tick representing 10%, *T. Index*, calculated conductivity, aridity (Dim1 and K/Ti), productivity (Dim2, Ca/Mg, Si/Zr, Sr/Ti, and inc/coh), and anoxia indices (Dim3, Mo, and Fe/Mn). Previous reconstruction from Cohen et al. (1983) is also included. Global climate phases are highlighted with the anticipated dry phase (Last Glacial Maximum, LGM) and the anticipated wet phase in blue (Bølling–Allerød interstadial, B-A). (For interpretation of the references to color in this figure legend, the reader is referred to the Web version of this article.)

5.2.5. Zone 4 – deeper, anoxic lake – 19.5 to 17.5 ka, 5.45–4.75 m

Zone 4 (19.5–17.5 ka, 5.45–4.75 m), like Zones 6 and 8, indicates anoxia, high productivity and organic content, and increased weathering (Fig. 8). The *T. Index* increases between Zones 5 and 4, signaling that this high *Thalassiosira rudolfi*/speckled green clay-phase is the result of increased depth and dilution, potentially more so than Zones 6 and 8. The decreased benthic taxa; increased planktonic taxa, including a spike in the deep freshwater-preference taxa *Aulacoseira granulata*; increased Dim1; and decreased K/Ti support this conclusion.

This wet phase from 19.5–17.5 ka matches well with a wet phase at Lake Masoko from 18.7–17.2 ka (Barker et al., 2003); at Chew Bahir after ~19 ka until the Younger Dryas, with the most rapid rise in moisture ~18 ka (Foerster et al., 2012); and at Lake Tanganyika from ~19–17.5 ka with a slight decrease in δD (Tierney et al., 2008) (Fig. 7), although records of increased biogenic silica and Rb/K seem to show this phase more clearly (Burnett et al., 2011). At the Burundi Highlands (Bonnefille and Chalié, 2000), Rutundu (Garellick et al., 2021), and Lake Chala (Verschuren et al., 2009), no wet phase is evident.

5.2.6. Zone 3 – highly alkaline lake – 17.5 to 15.4 ka, 4.75–3.55 m

Zone 3 (17.5–15.4 ka, 4.75–3.55 m) is composed of finely laminated soft green clays with short roots, indicating shallow and anoxic conditions. The laminations are composed almost exclusively of *Stephanocyclus meneghinianus* (Fig. 8), resulting in a conductivity of 4600 μS/cm and pH of 8.8 – the highest across the entire core. Such saline water could be chemically stratified, as evidenced at Nasikie Engida in the South Kenya Rift where high salinity prevents wind-induced disturbance in waters only 1–2 m deep (Renaut et al., 2021). Despite the color change, anoxic indicators are not particularly high (Fig. 8). Primary productivity increases after 16.5 ka, including that of diatoms (Si/Zr and diatom concentration (Fig. 6)) and cyanobacteria (Sr/Ti) which tend to prefer shallower, highly alkaline waters (Grant et al., 2006). At ~15.9 ka, several planktonic-rich layers indicate short-term deepening followed by a decrease in diatom productivity and inc/coh as well as an

increase cyanobacteria productivity (Fig. 8), indicating shallowing conditions until a surface layer at ~15.4 ka. The K/Ti and Dim1 record indicate that despite phases of weathered input, the water was still quite alkaline with substantial illitization of clays.

This zone matches a desiccation at Lake Victoria (Stager et al., 2002), with phases of desiccation and refilling of the basin >16.7 ka followed by expanding wetlands until 14.5 ka (Wienhues et al., 2023). At Chew Bahir, this timeframe appears to be a more stable dry phase before the start of the AHP (Foerster et al., 2012). Conditions appear to dry during this phase at Lake Tanganyika (Tierney et al., 2008), Lake Chala within the δD record (Tierney et al., 2011), and Lakes Masoko (Barker et al., 2003) and Rukwa (Barker et al., 2002) where there are hiatuses in the record (Fig. 7). The records from the Burundi Highlands (Bonnefille and Chalié, 2000) and Rutundu (Garellick et al., 2021) are less clear (Fig. 7).

5.2.7. Zone 2 – gradual deepening – 15.4 ka to unknown, 3.55–0.8 m

Zone 2 (15.4–Unknown, 3.55–0.8 m) represents a variety of sediments including fine sands, tephras, and green and brown clays with white diatom layers and high organic content (Fig. 2). This zone contains uncertainties in the age model due to potential hiatuses above 1.25 m (Table 1). We interpret the abrupt transition at ~3.09 m from sands to clays to indicate a hiatus. In our age model, this resulted in a ~300 yr hiatus which could be explained due to faulting activity or a mass-wasting event. Regardless, this section is interpreted as the AHP given the age of ~15 ka at 3.35 m and the high accumulation rate after 14 ka (~13 yr/cm) (Fig. 3).

The AHP is evident in nearly all the lakes across the EARS, particularly after the Younger Dryas 12.9–11.7 ka, at Lakes Turkana, Elmenteita, Nakuru, Naivasha, Magadi, Rukwa, Chad (Butzer et al., 1972; Cohen and Nielsen, 1986); Lake Chesi (Stager, 1988); Chew Bahir (Foerster et al., 2012); Paleolake Suguta (Garcin et al., 2009; Junginger et al., 2014); Lake Albert (Harvey, 1976); Lake Chala (Verschuren et al., 2009), Lake Masoko (Barker et al., 2003; Garcin et al., 2007), and Lake Victoria (Wienhues et al., 2023) (Fig. 7).

5.2.7.1. Zone 2a – variable lake – 15.4 to 13.6 ka, 3.55–2.6 m. Zone 2a (15.4–13.6 ka, 3.55–2.6 m) includes unlaminated soft, green clays that are topped by a black layer at 3.45 m. There is then a transition into dense, green clayey sands until 3.09 m. An uneven surface above the sands indicates a hiatus before organic-rich brown, slightly banded clayey silts. After a 3-cm thick ash layer at 2.88 m, the banding of the silts widens (Fig. 2). Given an age of $15,091 \pm 166$ at 3.35 m, the sands are interpreted as the beginning of the AHP. The larger grain size, however, biases the μ -XRF and diatom data: with rapid changes across the former and low concentration and increase in aerophilic taxa in the latter (Fig. 6), suggesting substantial allochthonous input (Davies et al., 2015) and diatom dissolution (Ryves et al., 2001; Flower and Ryves, 2009). Because of this, the high percentage of *Thalassiosira rudolfi* is not interpreted as earlier anoxic sections, particularly given the high species richness (Fig. 6) and lack of evidence for anoxia (Fig. 8). The shift from *T. rudolfi* to freshwater *Aulacoseira* spp. indicates wetter conditions by ~14.3 ka. The transition to wetter conditions may correlate with an increase in *A. granulata* and *Thalassiosira* spp. ~15.5–13.5 ka from Richardson and Dussinger (1986). Between the two cores, Richardson & Dussinger may represent a slightly deeper part of the lake with less mixing (Fig. 1). Other proxies also signal wetter conditions during deposition of the banded brown clays, including a decrease in Dim1 and K/Ti, and increased productivity, including an increase in Dim2, Ca/Mg, and Sr/Ti (Fig. 8).

5.2.7.2. Zone 2b – less variable lake – 13.6 to 12.6 ka, 2.55–1.65 m. Zone 2b (13.6–12.6 ka, 2.55–1.65 m) is more stable than the earlier phase of the AHP, with laminated organic-rich silt with light-colored laminae of varying widths, which turn into clayey silt with dark-colored bands (Fig. 2). The upper sediments are displaced by 1-cm by a normal fault. This subzone indicates high productivity and organic matter (Ca/Mg, Sr/Ti, and Dim2) and heavily weathered sediments (Dim1) (Fig. 8). The T. Index indicates deeper conditions than subzone 2a with *Aulacoseira granulata* var. *angustissima* (Müller) Simonsen potentially mirroring the *Aulacoseira* spp. zone of Richardson and Dussinger (1986) which ends ~12.1 ka. After this zone, the reliability of our age model decreases.

5.2.7.3. Zone 2c – loss of record – <12.6 ka to unknown, 1.65–0.8 m. Zone 2c (<12.6 ka–Unknown, 1.65–0.8 m) covers only 85 cm, similar to other AHP strata across the Naivasha and Nakuru-Elmenteita basins (Bergner et al., 2009). The lithology remains similar to Zone 2b, with organic-rich brown clayey silts and a 5-cm sand containing larger gravels at 1.54 m. The small fault from 1.54–2.15 m ends in this layer, indicating a faulting event prior or during the deposition of the sands. Due to the younger ages above the sand, we hypothesize a large mass wasting event occurred between 12.6 and 6 ka, probably due to faulting (Figs. 1 and 2). A pronounced change in many chemical parameters (Figs. 4 and 6) supports this assumption. Richardson and Dussinger (1986) (Fig. 2) observe a dominance of *Stephanodiscus* spp. at ~9.6 ka, representing substantially fresher and deeper waters than those observed at NAK. Interestingly, the Richardson and Dussinger (1986) core is also missing sediments above and below the *Stephanodiscus* zone, hinting at large-scale filling of the basin and/or one or two erosional events that removed sediments. Given the loss of sediments in this zone, interpretations are limited.

5.2.8. Zone 1 – post AHP heavily bioturbated – unknown, 0–0.8 m

Zone 1 (0–0.8 m) represents muds during historic deposition where bioturbation is likely (Fig. 2). This zone consists mostly of *Pantocsekia oscellata*, *Pseudostaurosira brevistriata*, *Aulacoseira muzzanensis* (Meister) Krammer, and *Cyclostephanos dubius* (Hustedt) Round, the latter two of which were not evident in such high percentages across the rest of the core (Fig. 6). This zone was calculated as the freshest, with a conductivity of ~700 and a pH of 7.7, which is very different from modern conditions (Renaut and Owen, 2023), indicating substantial mixing.

5.3. The impact of DO and H events on East African lakes

While precessional forcing's role in controlling hydroclimate is evident across the EARS (e.g., Kutzbach and Street-Perrott, 1985; Garcin et al., 2006; Foerster et al., 2012; Junginger et al., 2014, Fig. 7), few climate records, especially in the eastern branch, exist earlier than 25 ka. Therefore, despite records from the western branch and southeastern Africa often reflecting contrasting climate regimes to eastern branch records (e.g., Baker, 2002; Garcin et al., 2006; Tierney et al., 2008; Otto-Btiesner et al., 2014; Tian and Jiang, 2020), it is useful to utilize all records to better understand what contributes to hydroclimate across eastern Africa in the Pleistocene. Other hypotheses for what might control Pleistocene rainfall in eastern Africa include Indian Ocean SST (Tierney et al., 2008), the ENSO system (Tian and Jiang, 2020), and changes in Atlantic Meridional Overturning Circulation (AMOC) (Otto-Btiesner et al., 2014). While this review cannot support or refute these hypotheses, our high-resolution record, along with other records, may indicate AMOC's role, particularly suppression during a Heinrich event, in impacting rainfall in eastern Africa before the AHP. In the future, this could be further analyzed with higher quality age control, not just at NAK, but across the EARS.

Lake Nakuru's record may highlight the importance of SST and high- and low-latitude teleconnections on eastern African rainfall over the past 35 kyr on a centennial scale, particularly the Heinrich events (Holmgren et al., 2003; Trauth et al., 2018; Schaebitz et al., 2021). Through the last glacial (~115–11.7 ka), 30 short warming/cooling events have been observed in Greenland's ice cores (Huber et al., 2006, Fig. 7). A Dansgaard-Oeschger (DO) event, or Greenland Interstadial (Dansgaard et al., 1969, 1993), results in an 8–15°C increase over decades (Kindler et al., 2014). Temperatures then gradually cool until there is a rapid drop back to glacial temperatures called Heinrich (H) events, or Greenland Stadials (Heinrich, 1988). H events result in decreases in SST and salinity, with large calving events occurring over 6–8 kyr (Bond et al., 1992; Cimatoribus et al., 2013).

DO and H events impact global temperatures and moisture flux by impacting SST in the North Atlantic, ultimately impacting AMOC strength (Deplazes et al., 2014; Cheng et al., 2016), which has large impacts on the hydroclimate of the tropics, particularly related to the tropical rainbelt and monsoon strength (Sachs and Lehman, 1999). The clearest evidence of their tropical impact come from marine (e.g., Ivanochko et al., 2005; Itambi et al., 2009; Deplazes et al., 2013; Deplazes et al., 2014) and speleothem records (e.g., Wang et al., 2001; Holmgren et al., 2003; Fleitmann et al., 2009; Cheng et al., 2013; Cheng et al., 2016; Budsky et al., 2019). Along the Indo-Arabian coast, warmer SST during DO phases result in increased rainfall in eastern Africa similar to negative ENSO years, whereas during H events, freshwater input to the North Atlantic causes a decrease/shutdown of the AMOC, resulting in drier conditions (Deplazes et al., 2014). This appears to be supported by proxies across Africa (Nutz et al., 2024), and especially in eastern Africa where H events result in drier conditions (Stager et al., 2011; Foerster et al., 2012; Trauth et al., 2018), with response to DO events less clear. Ultimately, data from tropical lakes are lacking, especially those with high enough resolution and strong enough age models to note centennial-scale changes (Voelker, 2002).

Despite weak age control and often low data-resolution across the EARS, the synchronicity of brief wet and dry events across the EARS hints at these events' potential strength (Fig. 7 and references therein). Chew Bahir, which has the highest resolution, is incredibly variable and mirrors changes in the Arabian Sea and North Greenland ice sheet, with dry H events and wet DO events evident except at DO4 and DO2. The Tanganyika and Burundi Highland records are less clear, although in general it appears that H events are dry at these localities. DO events, which tend to be shorter, are more difficult to deduce in these records although at Tanganyika there appears to be a general wet phase from ~36–31 ka which includes DO5–7 and at ~15 ka with the start of DO1. The smoothed Burundi Highlands record results in resolution too low to

see DO events, although the unsmoothed data indicates there are short-term phases of wetter conditions including potential peaks around DO8, DO7, DO3, and DO1. The Nile Discharge record indicates dry phases during the H events, with less clarity during DO events. The Masoko record highlights the complication of looking at southern and northern EARS records together given the differing dynamics in rainfall. In general, the H events at Masoko appear dry (besides H4 which may have been overridden by a wet phase from DO8) with more complicated responses during DO events. In the Masoko record, it appears that DO8 and DO1 are wet, while the rest either are inconclusive or exhibit drier conditions. Of the shorter records, Lake Tana has low resolution where the majority of H and DO events are not visible, except for a clear lowstand at H3; Rutundu indicates drier conditions during H events and wetter conditions at DO1; Lake Chala indicates drier conditions across all H events and wetter conditions at all DO events; and Lake Rukwa indicates dry conditions at H1, with the higher moisture availability unclear due to the limitations of the diatom transfer function.

For comparison to other records, the median and ghost plot of Dim1 for NAK were plotted (Fig. 7) to more appropriately display uncertainties in our data and age model. In general, at NAK, the dry conditions of H events are evident whereas DO events are muddled by age model uncertainties. Both H2 and H1 are clear in NAK's ghost plot, with a rapid drying at Nakuru at 24 ka coincident with H2 and from 17.5–15.4 ka that straddles H1 (~16.7 ka (Hemming, 2004)). Between H1 and the Younger Dryas, the Lake Nakuru record does appear to reflect wetter conditions, that might, with a more refined age model, indicate a moisture spike at DO1. Similarly, the wet phase at the beginning of the record near the Menengai Tuff may match well with DO7 (Fig. 5). Overall, our high-resolution record, while indicating long-term zones of wet and dry phases on millennial scales, also represents substantial variability on centennial scales that, when compared to other records across the EARS, highlight potential for high latitude SST impact on low latitude moisture availability across eastern Africa.

6. Conclusions

As a closed basin at one of the highest points of the EARS, Lake Nakuru shows significant changes in hydrodynamics over the past 35 kyr. Past research has utilized Lake Nakuru's record to explain rift-wide climatic changes, like the AHP, but studying Lake Nakuru at high-resolution provides insights into a unique record with incredible sensitivity and minimal external input. Using lithological, diatom, TN, TC, TOC, WC, and μ -XRF element intensity data, this study uncovered millennial scale changes in climate that are not fully represented by diatom conductivity and pH transfer functions. This record highlights the local rate of change into the AHP with a highly alkaline phase from ~17.5–15.4 ka, leading into a wetter AHP that began with slightly variable wet conditions ~15.4–13.6 ka and more stable wet conditions ~13.6–12.6 ka. Over the past 35 kyr at Lake Nakuru, anoxic clays with low species richness and abundant *Thalassiosira rudolfi* (a high conductivity/pH preference taxa) ~35, ~25.5–24.5, and ~19.5–17.7 ka reflect highly productive and/or deeper waters with limited mixing over 1–2 kyr-timescales. Longer term records of shallow waters with phases of desiccation occur after ~35 ka and between ~24.5 and 19.7 ka. These millennial-scale changes include variability on centennial scales that may reflect potential teleconnections between high-latitude SST and African rainfall during the Late Pleistocene across the EARS.

Author contributions

Fieldwork and early analyses were conducted by A.B., M.T., and A.J. V.K., A.J. and E.R. contributed to core descriptions and reorganization. E.R. primarily prepared, conducted, analyzed, and interpreted the work related to diatoms, μ -XRF data, and the age model under the supervision of A.J. E.R. took the lead in writing the manuscript with critical feedback from C.R., S.K., A.J., and M.T. that helped shape the research, analysis,

and manuscript.

Declaration of competing interest

The authors declare that they have no known competing financial interests or personal relationships that could have appeared to influence the work reported in this paper.

Acknowledgements and Funding

We are grateful to the Government of Kenya and the Kenya Wildlife Service for research permits and support during the 2004 field season. Thank you to Lisa Park Boush, Ran Feng, and Christian Tryon for their help in early edits and discussions of these data. Thank you to the two anonymous reviewers that provided critical feedback on this work. Thank you to Tatiana Miranda for help on the SEM. Open Access funding enabled and organized by Projekt DEAL. E.R. acknowledges 2017 Fulbright Funding which began this project collaboration and an Outstanding Scholar Research Grant from the University of Connecticut that allowed the collaboration to continue. Original fieldwork was funded to M.T. by the German Research Foundation (DFG) TR419/3-1 titled "The Lake Naivasha Coring Project". E.R. would also like to acknowledge current funding through the HESCOR (Human and Earth Systems Coupled Research) project which is part of the "Profile Building 2022" initiative by North Rhine-Westphalia's Ministry for Culture and Science. This research is also part of "Wet Feet or Walking on Sunshine" awarded to A.J., funded by the Ministry of Culture and Science (MWK) of Baden-Württemberg, the University of Tübingen, and Senckenberg Centre for Human Evolution and Paleoenvironment, Germany. C.R. acknowledges funding from the Excellence Strategy Initiative of the State of Baden-Württemberg and University of Tübingen for the Project CLASH, and Grant PTA2022-021985-I funded by MCIN/AEI/10.13039/501100011033 and by ESF+.

Appendix A. Supplementary data

Supplementary data to this article can be found online at <https://doi.org/10.1016/j.quascirev.2025.109579>.

Data availability

A link to the data and/or code is provided as part of this submission.

References

- Altabet, M.A., Higginson, M.J., Murray, D.W., 2002. The effect of millennial-scale changes in Arabian Sea denitrification on atmospheric CO₂. *Nature* 415, 159–162.
- Ambrose, S.H., Sikes, N.E., 1991. Soil carbon isotope evidence for Holocene habitat change in the Kenya Rift Valley. *Science* 253 (5026), 1402–1405.
- Ambrose, S.H., 1984. Holocene Environments and Human Adaptations in the Central Rift Valley, Kenya. University of California, Berkeley. PhD Thesis.
- Arbuszewski, J.A., deMenocal, P.B., Cléroux, C., Bradtmiller, L., Mix, A., 2013. Meridional shifts of the Atlantic intertropical convergence Zone since the last glacial maximum. *Nat. Geosci.* 6 (11), 959–962. <https://doi.org/10.1038/ngeo1961>.
- Baker, B.H., 1986. Tectonics and volcanism of the southern Kenya Rift Valley and its influence on rift sedimentation. *Geol. Soc. Lond. Spec. Publ.* 25, 45–57. <https://doi.org/10.1144/GSL.SP.1986.025.01.05>.
- Baker, P.A., 2002. Trans-Atlantic climate connections. *Science* 296 (5565), 67–68.
- Baker, B.H., Wohlenberg, J., 1971. Structure and evolution of the Kenya rift Valley. *Nature (London)* 229 (5286), 538–542. <https://doi.org/10.1038/229538a0>.
- Baker, B.H., Mitchell, J.G., William, L.A.J., 1988. Stratigraphy, geochronology and volcano-tectonic evolution of the kedong-naivasha-kinangop Region, gregory Rift Valley, Kenya. *J. Geol. Soc.* 145 (1), 107–116. <https://doi.org/10.1144/gsjgs.145.1.0107>.
- Ballot, A., Krienitz, L., Kotut, K., Wiegand, C., Metcalf, J.S., Codd, G.A., Pflugmacher, S., 2004. Cyanobacteria and cyanobacterial toxins in three alkaline Rift Valley Lakes of Kenya—Lakes Bogoria, Nakuru and Elmenteita. *J. Plankton Res.* 26 (8), 925–935. <https://doi.org/10.1093/plankt/fbh084>.
- Barker, P.A., Talbot, M.R., Street-Perrott, F., Marret, F., Scourse, J., Odada, E.O., 2004. Late Quaternary climatic variability in intertropical Africa. In: Battarbee, R.W., Gasse, F., Stickley, C.E. (Eds.), *Past Climate Variability Through Europe and Africa*. Springer Netherlands, Dordrecht, pp. 117–138.

- Barker, P., Telford, R., Gasse, F., Thevenon, F., 2002. Late Pleistocene and Holocene palaeohydrology of Lake Rukwa, Tanzania, inferred from diatom analysis. *Palaeogeogr. Palaeoclimatol. Palaeoecol.* 187 (3), 295–305. [https://doi.org/10.1016/S0031-0182\(02\)00482-0](https://doi.org/10.1016/S0031-0182(02)00482-0).

Barker, P., Williamson, D., Gasse, F., Gibert, E., 2003. Climatic and volcanic forcing revealed in a 50,000-Year diatom record from Lake massoko, Tanzania. *Quat. Res.* 60 (3), 368–376. <https://doi.org/10.1016/j.yqres.2003.07.001>.

Battarbee, R.W., 1986. Diatom analysis. In: Berglund, B.E. (Ed.), *Handbook of Holocene Palaeoecology & Palaeohydrology*, pp. 527–570.

Battarbee, R.W., Juggins, S., Gasse, F., Anderson, N.J., Bennion, H., Cameron, N.G., Ryves, D.B., Pailles, C., Chalie, F., Telford, R., 2001. European diatom database (EDDI). an information system for palaeoenvironmental reconstruction. *ECRC Research Report* 81, 1–94.

Bergner, A.G.N., Trauth, M.H., Bookhagen, B., 2003. Paleoprecipitation estimates for the Lake Naivasha Basin (Kenya) during the last 175 K.Y. using a Lake-Balance Model. *Global Planet. Change* 36 (1), 117–136. [https://doi.org/10.1016/S0921-8181\(02\)00178-9](https://doi.org/10.1016/S0921-8181(02)00178-9).

Bergner, A.G.N., Strecker, M.R., Trauth, M.H., Deino, A., Gasse, F., Blisniuk, P., Dühnforth, M., 2009. Tectonic and climatic control on evolution of Rift Lakes in the central Kenya Rift, East Africa. *Quat. Sci. Rev.* 28 (25), 2804–2816. <https://doi.org/10.1016/j.quascirev.2009.07.008>.

Birks, H.J.B., Heiri, O., Seppä, H., Bjune, A.E., 2010. Strengths and weaknesses of quantitative climate reconstructions based on late-quaternary biological proxies. *Quat. Int.* 279–280. <https://doi.org/10.1016/j.quaint.2012.07.228>.

Blaauw, M., Christen, J.A., 2011. Flexible paleoclimate age-depth models using an autoregressive gamma process. *Bayesian Analysis* 6 (3), 457–474. <https://doi.org/10.1214/ba/1339616472>.

Blegen, N., Brown, F.H., Jicha, B.R., Binetti, K.M., Faith, J.T., Ferraro, J.V., Gathogo, P. N., Richardson, J.L., Tryon, C.A., 2016. The menengai tuff: a 36 Ka widespread tephra and its chronological relevance to late Pleistocene human evolution in East Africa. *Quat. Sci. Rev.* 152, 152–168. <https://doi.org/10.1016/j.quascirev.2016.09.020>.

Bond, G., Heinrich, H., Broecker, W., Labeyrie, L., McManus, J., Andrews, J., Huon, S., et al., 1992. Evidence for massive discharges of icebergs into the North Atlantic Ocean during the last glacial period. *Nature (London)* 360 (6401), 245–249. <https://doi.org/10.1038/360245a0>.

Bonnefille, R., Chalié, F., 2000. Pollen-Inferred precipitation time-series from equatorial Mountains, Africa, the last 40 Kyr BP. *Global Planet. Change* 26 (1), 25–50. [https://doi.org/10.1016/S0921-8181\(00\)00032-1](https://doi.org/10.1016/S0921-8181(00)00032-1).

Bosworth, W., Strecker, M.R., 1997. Stress field changes in the Afro-Arabian rift system during the Miocene to Recent period. *Tectonophysics* 278 (1–4), 47–62.

Braconnot, P., Marzin, C., Grégoire, L., Mosquet, E., Marti, O., 2008. Monsoon response to changes in Earth's orbital parameters: comparisons between simulations of the eemian and of the Holocene. *Clim. Past* 4 (4), 281–294. <https://doi.org/10.5194/cp-4-281-2008>.

Brauer, A., 2004. Annually laminated Lake sediments and their palaeoclimatic relevance. *The Climate in Historical Times: towards a Synthesis of Holocene Proxy Data and Climate Models*, pp. 109–127.

Brindle, M., Mohan, J., Beck, C., Stone, J.R., 2018. Three novel species of bacillariophyta (Diatoms) in the genera *surrella* and *thalassiosira* from Pleistocene paleolake Lorenyeng (\sim 2 - 1.6 ma) Turkana Basin, Kenya. *Phytotaxa* 371 (3), 230. <https://doi.org/10.11646/phytotaxa.371.36>.

Broecker, W.S., Putname, A.E., 2013. Hydrologic impacts of past shifts of Earth's thermal equator offer insight into those to be produced by fossil fuel CO₂. *Proc. Natl. Acad. Sci. USA* 110 (42), 16710–16715. <https://doi.org/10.1073/pnas.1301855110>.

Brothers, S., Köhler, J., Attermeyer, K., Grossart, H.P., Mehner, T., Meyer, N., Scharnweber, K., Hilt, S., 2014. A feedback loop links brownification and anoxia in a temperate, shallow Lake. *Limnol. Oceanogr.* 59 (4), 1388–1398. <https://doi.org/10.4319/lo.2014.59.4.1388>.

Budsky, A., Wassenburg, J.A., Mertz-Kraus, R., Spötl, C., Jochum, K.P., Gibert, L., Scholz, D., 2019. Western mediterranean climate response to dansgaard/oeschger events: new insights from speleothem records. *Geophys. Res. Lett.* 46 (15), 9042–9053. <https://doi.org/10.1029/2019GL084009>.

Burnett, A.P., Soreghan, M.J., Scholz, C.A., Brown, E.T., 2011. Tropical East African climate change and its relation to global climate: a record from Lake Tanganyika, tropical East Africa, over the past 90+ kyr. *Palaeogeogr. Palaeoclimatol. Palaeoecol.* 303 (1), 155–167. <https://doi.org/10.1016/j.palaeo.2010.02.011>.

Butzer, K.W., Isaac, G.L., Richardson, J.L., Washbourn-Kamau, C., 1972. Radiocarbon dating of East African Lake levels. *Science* 175 (4026), 1069–1076.

Cambrani, P., 1997. Rainfall anomalies in the source Region of the Nile and their connection with the Indian summer monsoon. *J. Clim.* 10, 1380–1392. [https://doi.org/10.1175/1520-0442\(1997\)010](https://doi.org/10.1175/1520-0442(1997)010).

Cantonati, M., Scola, S., Angelini, N., Guella, G., Frassanito, R., 2009. Environmental controls of epilithic diatom depth-distribution in an oligotrophic Lake characterized by marked water-level fluctuations. *Eur. J. Phycol.* 44 (1), 15–29. <https://doi.org/10.1080/09670260802079335>.

Chase, Brian M., Boom, Arnoud, Carr, Andrew S., Reimer, Paula J., 2022. Climate variability along the Margin of the Southern African monsoon Region at the end of the African humid period. *Quat. Sci. Rev.* 291 (September), 107663. <https://doi.org/10.1016/j.quascirev.2022.107663>.

Cheng, H., Edwards, R.L., Sinha, A., Spötl, C., Yi, L., Chen, S., Kelly, M., et al., 2016. The Asian monsoon over the past 640,000 years and ice age terminations. *Nature (London)* 534 (7609), 640–646. <https://doi.org/10.1038/nature18591>.

Cheng, H., Sinha, A., Cruz, F.W., Wang, X., Edwards, R.L., D'Horta, F.M., Ribas, C.C., Vuille, M., Stott, L.D., Adler, A.S., 2013. Climate change patterns in Amazonia and biodiversity. *Nat. Commun.* 4 (1411). <https://doi.org/10.1038/ncomms2415>.

Cimatoribus, A.A., Drijfhout, S.S., Livina, V., van der Schrier, G., 2013. Dansgaard-oeschger events: bifurcation points in the climate system. *Clim. Past* 9 (1), 323–333. <https://doi.org/10.5194/cp-9-323-2013>.

Clark, P.U., Dyke, A.S., Shakun, J.D., Carlson, A.E., Clark, J., Wohlfarth, B., Mitrovica, J. X., Hostetler, S.W., McCabe, A.M., 2009. The last glacial maximum. *Science* 325 (5941), 710–714. <https://doi.org/10.1126/science.1172873>.

Clarke, M.C.G., Woodhall, D.G., Allen, D., Darling, G., 1990. "Geological, volcanological and hydrogeological controls on the occurrence of geothermal activity in the area surrounding Lake Naivasha, Kenya.". British Geological Survey Report and Government of Kenya—Ministry of Energy, Nairobi, Kenya.

Cocquyt, C., 1998. Diatoms from the Northern Basin of Lake Tanganyika. *J. Cramer, Berlin*.

Cocquyt, C., Verschuren, D., 2023. Checklist of the diatoms from Lake Naivasha, Kenya, with some historical notes. *PhytoKeys* 224 (1), 101–174. <https://doi.org/10.3897/phytokeys.224.98168>.

Cohen, A.S., Dussinger, R., Richardson, J., 1983. Lacustrine paleochemical interpretations based on Eastern and Southern African ostracodes. *Palaeogeogr. Palaeoclimatol. Palaeoecol.* 43 (1), 129–151. [https://doi.org/10.1016/0031-0182\(83\)90051-2](https://doi.org/10.1016/0031-0182(83)90051-2).

Cohen, A.S., Nielsen, C., 1986. Ostracodes as indicators of paleohydrochemistry in Lakes: a late Quaternary example from Lake elmenteita, Kenya. *Palaios* 1 (6), 601–609. <https://doi.org/10.2307/3514710>.

Cole, S., 1963. *The Prehistory of East Africa*. Macmillan, New York.

Conti, P., Pistis, M., Bernardinetti, S., Barbagli, A., Zirulia, A., Serri, L., Colonna, T., Guastaldi, E., Ghiglieri, G., 2021. Tectonic setting of the Kenya rift in the Nakuru area, based on geophysical prospecting. *Geosciences (Basel)* 11 (2), 80. <https://doi.org/10.3390/geosciences11020080>.

Crema, E.R., Bevan, A., 2021. Inference from large sets of radiocarbon dates: software and methods. *Radiocarbon* 63, 23–39. <https://doi.org/10.1017/RDC.2020.95>.

Dansgaard, W., Johnsen, S.J., Clausen, H.B., Dahl-Jensen, D., Gundestrup, N.S., Hammer, C.H., Hvidberg, C.S., et al., 1993. Evidence for general instability of past climate from a 250-Kyr ice-core record. *Nature (London)* 364 (6434), 218–220. <https://doi.org/10.1038/364218a0>.

Dansgaard, W., Johnsen, S.J., Møller, J., Langway, C.C., 1969. One thousand centuries of climatic record from camp century on the Greenland ice sheet. *Science* 166 (3903), 377–381. <https://doi.org/10.1126/science.166.3903.377>.

Davies, S.J., Lamb, H.F., Roberts, S.J., 2015. Micro-XRF core scanning in palaeolimnology: recent developments. In: Croudace, I.W., Rothwell, R.G. (Eds.), *Micro-XRF Studies of Sediment Cores*, 17. Springer, pp. 189–226.

De Cort, G., Bessem, I., Keppens, E., Mees, F., Cumming, B., Verschuren, D., 2013. Late-holocene and recent hydroclimatic variability in the central Kenya Rift Valley: the sediment record of hypersaline Lakes Bogoria, Nakuru and elementeita. *Palaeogeogr. Palaeoclimatol. Palaeoecol.* 388, 69–80. <https://doi.org/10.1016/j.palaeo.2013.07.029>.

deMenocal, P.B., 1995. Plio-Pleistocene African climate. *Science* 270 (5233), 53–59. <https://doi.org/10.1126/science.270.5233.53>.

deMenocal, Peter, Ortiz, Joseph, Guilderson, Tom, Adkins, Jess, Sarnthein, Michael, Baker, Linda, Yarusinsky, Martha, 2000. Abrupt onset and termination of the African humid period: rapid climate responses to gradual insolation forcing. *Quat. Sci. Rev.* 19 (1), 347–361. [https://doi.org/10.1016/S0277-3791\(99\)00081-5](https://doi.org/10.1016/S0277-3791(99)00081-5).

Deplazes, G., Lückge, A., Peterson, L.C., Timmermann, A., Hamann, Y., Hughen, K.A., Röhli, U., et al., 2013. Links between tropical rainfall and north Atlantic climate during the last glacial period. *Nat. Geosci.* 6 (3), 213–217. <https://doi.org/10.1038/ngeo1712>.

Deplazes, G., Lückge, A., Stuut, J.-B.W., Pätzold, J., Kuhlmann, H., Husson, D., Fant, M., Haug, G.H., 2014. Weakening and strengthening of the Indian monsoon during heinrich events and dansgaard/oeschger oscillations. *Paleoceanography* 29 (2), 99–114. <https://doi.org/10.1002/2013PA002509>.

Duesing, Walter, Kaboth-Bahr, Stefanie, Asrat, Asfawossen, Cohen, Andrew S., Foerster, Verena, Lamb, Henry F., Schaebitz, Frank, Trauth, Martin H., Viebahn, Finn, 2021. Changes in the cyclicity and variability of the Eastern African paleoclimate over the last 620 kyr. *Quat. Sci. Rev.* 273 (December), 107219. <https://doi.org/10.1016/j.quascirev.2021.107219>.

Duggen, S., Olgun, N., Croot, P., Hoffmann, L., Dietze, H., Delmelle, P., Teschner, C., 2010. The role of airborne volcanic ash for the surface ocean biogeochemical iron-cycle: a review. *Biogeosciences* 7 (3), 827–844. <https://doi.org/10.5194/bg-7-827-2010>.

Dühnforth, M., Bergner, An G.N., Trauth, M.H., 2006. Early Holocene water budget of the Nakuru-Elmenteita Basin, central Kenya rift. *J. Paleolimnol.* 36 (3), 281–294. <https://doi.org/10.1007/s10933-006-9003-z>.

Egborge, A.B.M., 1979. The effect of impoundment on the water chemistry of Lake asejire, Nigeria. *Freshw. Biol.* 9 (5), 403–412. <https://doi.org/10.1111/j.1365-2427.1979.tb01525.x>.

Ehrmann, W., Schmidli, G., Seidel, M., Krüger, S., Schulz, H., 2016. A distal 140 kyr sediment record of Nile discharge and east African monsoon variability. *Clim. Past* 12 (3), 713–727. <https://doi.org/10.5194/cp-12-713-2016>.

Fazi, S., Butturini, A., Tassi, F., Amalfitano, S., Venturi, S., Vazquez, E., Clokie, M., Wanjala, S.W., Pacini, N., Harper, D.M., 2018. Biogeochemistry and biodiversity in a network of saline-alkaline Lakes: implications of ecohydrological connectivity in the Kenyan rift Valley. *Ecohydrobiol. Hydrobiol.* 18 (2), 96–106. <https://doi.org/10.1016/j.ecohyd.2017.09.003>.

Fleitmann, D., Cheng, H., Badertscher, S., Edwards, R.L., Mudelsee, M., Göktürk, O.M., Fankhauser, A., et al., 2009. Timing and climatic impact of Greenland interstadials recorded in stalagmites from Northern Turkey. *Geophys. Res. Lett.* 36 (19), L19707-n/a. <https://doi.org/10.1029/2009GL040050>.

- Flint, R.F., 1959a. On the basis of Pleistocene correlation in East Africa. *Geol. Mag.* 96 (4), 265–284. <https://doi.org/10.1017/S0016756800060751>.
- Flint, R.F., 1959b. Pleistocene climates in Eastern and Southern Africa. *Bull. Geol. Soc. Am.* 70 (3), 343–373. [https://doi.org/10.1130/0016-7606\(1959\)70](https://doi.org/10.1130/0016-7606(1959)70).
- Flower, R.J., Ryves, D.B., 2009. Diatom preservation: differential preservation of sedimentary diatoms in two saline Lakes. *Acta Bot. Croat.* 68 (2), 381–399.
- Foerster, V., Asrat, A., Ramsey, C.B., Brown, E.T., Chapot, M.S., Deino, A., Duesing, W., Grove, M., Hahn, A., Junginger, A., 2022. Pleistocene climate variability in Eastern Africa influenced hominin evolution. *Nat. Geosci.* 15 (10), 805–811.
- Foerster, V., Deocampo, D.M., Asrat, A., Günter, C., Junginger, A., Krämer, K.H., Stroncik, N.A., Trauth, M.H., 2018. Towards an understanding of climate proxy formation in the chew Bahir Basin, Southern Ethiopian rift. *Palaeogeogr. Palaeoclimatol. Palaeoecol.* 501, 111–123. <https://doi.org/10.1016/j.palaeo.2018.04.009>.
- Foerster, V., Junginger, A., Langkamp, O., Gebru, T., Asrat, A., Umer, M., Lamb, H.F., et al., 2012. Climatic change recorded in the sediments of the Chew Bahir Basin, Southern Ethiopia, during the last 45,000 years. *Quat. Int.* 274, 25–37. <https://doi.org/10.1016/j.quaint.2012.06.028>.
- Garcin, Y., Junginger, A., Melnick, D., Olago, D.O., Strecker, M.R., Trauth, M.H., 2009. Late Pleistocene–Holocene rise and collapse of Lake suguta, Northern Kenya rift. *Quat. Sci. Rev.* 28 (9), 911–925. <https://doi.org/10.1016/j.quascirev.2008.12.006>.
- Garcin, Y., Vincens, A., Williamson, D., Buchet, G., Guiot, J., 2007. Abrupt resumption of the African monsoon at the younger dryas—holocene climatic transition. *Quat. Sci. Rev.* 26 (5), 690–704. <https://doi.org/10.1016/j.quascirev.2006.10.014>.
- Garcin, Y., Vincens, A., Williamson, D., Guiot, J., Buchet, G., 2006. Wet phases in tropical Southern Africa during the last glacial period. *Geophys. Res. Lett.* 33 (7), L07703–n/a. <https://doi.org/10.1029/2005GL025531>.
- Garellick, S., Russell, J.M., Dee, S., Verschuren, D., Olago, D.O., 2021. Atmospheric controls on precipitation isotopes and hydroclimate in high-elevation regions in eastern Africa since the last glacial maximum. *Earth Planet Sci. Lett.* 567, 116984. <https://doi.org/10.1016/j.epsl.2021.116984>.
- Gasse, F., Juggins, S., Khelifa, L.B., 1995. Diatom-based transfer functions for inferring past hydrochemical characteristics of African Lakes. *Palaeogeogr. Palaeoclimatol. Palaeoecol.* 117 (1), 31–54. [https://doi.org/10.1016/0031-0182\(94\)00122-O](https://doi.org/10.1016/0031-0182(94)00122-O).
- Gasse, F., 1986. East African Diatoms: Taxonomy, Ecological Distribution. *J. Cramer, Berlin*.
- Gasse, F., 2000. Hydrological changes in the African tropics since the last glacial maximum. *Quat. Sci. Rev.* 19 (1), 189–211. [https://doi.org/10.1016/S0277-3791\(99\)00061-X](https://doi.org/10.1016/S0277-3791(99)00061-X).
- Gasse, F., Barker, P., Gell, P.A., Fritz, S.C., Chalé, F., 1997. Diatom-inferred salinity in palaeolakes: an indirect tracer of climate change. *Quat. Sci. Rev.* 16 (6), 547–563. [https://doi.org/10.1016/S0277-3791\(96\)00081-9](https://doi.org/10.1016/S0277-3791(96)00081-9).
- Gasse, F., Barker, P., Johnson, T.C., 2002. A 24,000 Yr diatom record from the Northern Basin of Lake Malawi. *The East African Great Lakes: Limnology, Palaeolimnology and Biodiversity*, pp. 393–414.
- Gasse, F., Chalié, F., Vincens, A., Williams, M.A.J., Williamson, D., 2008. Climatic patterns in equatorial and Southern Africa from 30,000 to 10,000 years ago reconstructed from terrestrial and near-shore proxy data. *Quat. Sci. Rev.* 27 (25), 2316–2340. <https://doi.org/10.1016/j.quascirev.2008.08.027>.
- Giralt, S., Rico-Herrero, M.T., Vega, J.C., Valero-Garcés, B.L., 2011. Quantitative climate reconstruction linking meteorological, limnological and XRF core scanner datasets: the Lake Sanabria case study, NW Spain. *J. Paleolimnol.* 46 (3), 487–502. <https://doi.org/10.1007/s10933-011-9509-x>.
- Grant, W., Gerday, C., Glansdorff, N., 2006. Alkaline environments and biodiversity. In: *Extremophiles Volume, III*. EOLSS publishers, pp. 21–39.
- Gregory, J.W., 1968. The great rift Valley: being the narrative of a journey to Mount Kenya and Lake Baringo, with some account of the geology. *Natural History, Anthropology and Future Prospects of British East Africa*, first ed. London: Cass.
- Gregory, J.W., 1921. The Rift Valleys and Geology of East Africa; an Account of the Origin & History of the Rift Valleys of East Africa & their Relation to the Contemporary Earth-Movements which Transformed the Geography of the World. with Some Account of the Prehistoric Stone Implements, Soils, Water Supply, & Mineral Resources of the Kenya Colony. Seely, Service & Co. Limited, England.
- Griffith, Peter, 2020. Late Quaternary Palaeoenvironments and Middle-Late Stone Age Habitat Preferences in the Nakuru-Naivasha Basin, Kenya: Phytolith-Based Evidence from the Site of Prospect Farm. PhD Thesis. Darwin College.
- Halfman, J.D., Jacobson, D.F., Cannella, C.M., Haberyan, K.A., Finney, B.P., 1992. Fossil diatoms and the mid to late Holocene paleolimnology of Lake Turkana, Kenya: a reconnaissance Study. *J. Paleolimnol.* 7 (1), 23–35. <https://doi.org/10.1007/BF00197029>.
- Hare, L., Carter, J.C.H., 1984. Diel and seasonal physico-chemical fluctuations in a small natural west African Lake. *Freshw. Biol.* 14 (6), 597–610. <https://doi.org/10.1111/j.1365-2427.1984.tb00179.x>.
- Harvey, T.J., 1976. The Paleolimnology of Lake Mobutu Sese Seko, Uganda-Zaire: the Last 28,000 Years. Duke University.
- Hasle, G.R., 1978. Some freshwater and Brackish water species of the diatom Genus *Thalassiosira* cleve. *Phycologia* 17 (3), 263–292. <https://doi.org/10.2216/i0031-8884-17-3-263.1>.
- Hastenrath, S., Kutzbach, J.E., 1983. Paleoclimatic estimates from water and energy budgets of east African Lakes. *Quat. Res.* 19 (2), 141–153. [https://doi.org/10.1016/0033-5894\(83\)90001-7](https://doi.org/10.1016/0033-5894(83)90001-7).
- Hayashi, T., 2011. Monospecific planktonic diatom assemblages in the paleo-kathmandu Lake during the middle Brunhes chron: implications for the paradox of the plankton. *Palaeogeogr. Palaeoclimatol. Palaeoecol.* 300 (1–4), 46–58. <https://doi.org/10.1016/j.palaeo.2010.12.007>.
- Hecky, R.E., Bugenyi, F.W.B., Ochumba, P., Talling, J.F., Mugidde, R., Gophen, M., Kaufman, L., 1994. Deoxygenation of the deep water of Lake Victoria, East Africa. *Limnol. Oceanogr.* 39 (6), 1476–1481. <https://doi.org/10.4319/lo.1994.39.6.1476>.
- Heinrich, H., 1988. Origin and consequences of cyclic ice rafting in the Northeast Atlantic Ocean during the past 130,000 years. *Quat. Res.* 29 (2), 142–152. [https://doi.org/10.1016/0033-5894\(88\)90057-9](https://doi.org/10.1016/0033-5894(88)90057-9).
- Heinrich, S.R., 2004. Heinrich events: massive late Pleistocene detritus layers of the North Atlantic and their global climate imprint. *Rev. Geophys.* 42 (1), RG1005–n/a. <https://doi.org/10.1029/2003RG000128>, 1985.
- Herrnegger, M., Stecher, G., Schwatke, C., Olang, L., 2021. Hydroclimatic analysis of rising water levels in the great rift Valley Lakes of Kenya. *J. Hydrol.: Reg. Stud.* 36, 100857. <https://doi.org/10.1016/j.ejrh.2021.100857>.
- Hurons, L., Turner, A., 2018. The impact of Indian Ocean mean-state biases in climate models on the representation of the East African short rains. *J. Clim.* 31 (16), 6611–6631. <https://doi.org/10.1175/JCLI-D-17-0804.1>.
- Holmgren, K., Lee-Thorp, J., Cooper, G.R.J., Lundblad, K., Partridge, T.C., Scott, L., Sithaideen, R., Talma, A.S., Tyson, P.D., 2003. Persistent millennial-scale climatic variability over the past 25,000 years in Southern Africa. *Quat. Sci. Rev.* 22 (21), 2311–2326. [https://doi.org/10.1016/S0277-3791\(03\)00204-X](https://doi.org/10.1016/S0277-3791(03)00204-X).
- Huber, C., Leuenberger, M., Spahni, R., Flückiger, J., Schwander, J., Stocker, T.F., Johnsen, S., Landais, A., Jouzel, J., 2006. Isotope calibrated Greenland temperature record over marine isotope stage 3 and its relation to CH 4. *Earth Planet Sci. Lett.* 243 (3), 504–519. <https://doi.org/10.1016/j.epsl.2006.01.002>.
- Itambi, A.C., von Dobeneck, T., Mulitza, S., Bickert, T., Heslop, D., 2009. Millennial-scale Northwest African droughts related to Heinrich events and Dansgaard-Oeschger cycles: evidence in marine sediments from offshore Senegal. *Paleoceanography* 24 (1), PA1205–n/a. <https://doi.org/10.1029/2007PA001570>.
- IUSS Working Group, 2014. "World reference base for soil resources 2014. International Soil Classification System for Naming Soils and Creating Legends for Soil Maps.
- Ivanochko, T.S., Ganeshram, R.S., Brummer, G.-J.A., Ganssen, G., Jung, S.J.A., Moreton, S.G., Kroon, D., 2005. Variations in tropical convection as an amplifier of global climate change at the millennial scale. *Earth Planet Sci. Lett.* 235 (1), 302–314. <https://doi.org/10.1016/j.epsl.2005.04.002>.
- Jirska, F., Gruber, M., Stojanovic, A., Omondi, S.O., Mader, D., Körner, W., Schagerl, M., 2013. Major and trace element geochemistry of Lake Bogoria and Lake Nakuru, Kenya, during extreme draught. *Chem. Erde* 73 (3), 275–282. <https://doi.org/10.1016/j.chemer.2012.09.001>.
- Juggins, S., 2022. Rioja: analysis of Quaternary science data. R package version 1, 0–5.
- Junginger, A., 2006. Mikrofazielle Untersuchungen an laminierten Sedimenten des Lake Nakuru, Kenia. Institut für Geowissenschaften, University of Potsdam, Potsdam, Germany.
- Junginger, A., Roller, S., Olaka, L.A., Trauth, M.H., 2014. The effects of solar irradiation changes on the migration of the Congo air boundary and water levels of Paleo-Lake suguta, Northern Kenya rift, during the African humid period (15–5 Ka BP). *Palaeogeogr. Palaeoclimatol. Palaeoecol.* 396, 1–16. <https://doi.org/10.1016/j.palaeo.2013.12.007>.
- Junginger, A., Trauth, M.H., 2013. Hydrological constraints of paleo-lake suguta in the Northern Kenya rift during the African humid period (15–5 Ka BP). *Global Planet. Change* 111, 174–188. <https://doi.org/10.1016/j.gloplacha.2013.09.005>.
- Kanda, I.K., 2010. Aquifer Stratigraphy and Hydrogeochemistry of the Lake Nakuru Basin, Central Kenya Rift. University of Nairobi. Unpublished Dissertation.
- Kimaru, A.N., Gathenya, J.M., Cheruiyot, C.K., 2019. The temporal variability of rainfall and streamflow into Lake Nakuru, Kenya, assessed using SWAT and hydrometeorological indices. *Hydrology* 6 (4), 88. <https://doi.org/10.3390/hydrology6040088>.
- Kindler, P., Guillevic, M., Baumgartner, M., Schwander, J., Landais, A., Leuenberger, M., 2014. Temperature reconstruction from 10 to 120 Kyr B2k from the NGRIP ice core. *Clim. Past* 10 (2), 887–902. <https://doi.org/10.5194/cp-10-887-2014>.
- Kingston, John D., Hill, Andrew, 2005. When it rains it pours: legends and realities of the East African pluvials. In: *Interpreting the past*. Brill, pp. 189–205.
- Kniess, U., 2006. Hydrologische Modellierung im Zentralen Kenya-Rift. University of Potsdam. Unpublished Diploma Thesis.
- Kragh, T., Martensen, K.T., Kristensen, E., Sand-Jensen, K., 2020. From drought to flood: sudden carbon inflow causes whole-lake anoxia and massive fish kill in a large shallow Lake. *Sci. Total Environ.* 739, 140072. <https://doi.org/10.1016/j.scitotenv.2020.140072>.
- Kübler, S., Rucina, S., Reynolds, S., Owenga, P., Bailey, G., King, G., 2016. Edaphic and topographic constraints on exploitation of the Central Kenya Rift by large mammals and early hominins. *Open Quat.* 2, 1–18.
- Kuechler, R.R., Schefuß, E., Beckmann, B., Dupont, L., Wefer, G., 2013. NW African hydrology and vegetation during the last glacial cycle reflected in plant-wax-specific hydrogen and carbon isotopes. *Quat. Sci. Rev.* 82, 56–67. <https://doi.org/10.1016/j.quascirev.2013.10.013>.
- Kurenkov, I.I., 1966. The influence of volcanic ashfall on biological processes in a Lake. *Limnol. Oceanogr.* 11 (3), 426–429. <https://doi.org/10.4319/lo.1966.11.3.0426>.
- Kutzbach, J.E., Street-Perrott, F., 1985. Milankovitch forcing of fluctuations in the level of tropical Lakes from 18 to 0 Kyr BP. *Nature (London)* 317 (6033), 130–134. <https://doi.org/10.1038/317130a0>.
- Laird, K.R., Kingsbury, M.V., Cumming, B.F., 2010. Diatom habitats, species diversity and water-depth inference models across surface-sediment transects in worth Lake, Northwest Ontario, Canada. *J. Paleolimnol.* 44 (4), 1009–1024. <https://doi.org/10.1007/s10933-010-9470-0>.
- Laird, K.R., Kingsbury, M.V., Lewis, C.F.M., Cumming, B.F., 2011. Diatom-inferred depth models in 8 Canadian boreal Lakes: inferred changes in the benthic:planktonic depth boundary and implications for assessment of past droughts. *Quat. Sci. Rev.* 30 (9), 1201–1217. <https://doi.org/10.1016/j.quascirev.2011.02.009>.

- Lamb, H.F., Bates, C.R., Bryant, C.L., Davies, S.J., Huws, D.G., Marshall, M.H., Roberts, H.M., Toland, H., 2018. 150,000-Year palaeoclimate record from northern Ethiopia supports early, multiple dispersals of modern humans from Africa. *Sci. Rep.* 8 (1), 1077. <https://doi.org/10.1038/s41598-018-19601-w>.
- Leakey, L.S.B., 1931. East African Lakes. *Geogr. J.* 77 (6), 497–508. <https://doi.org/10.2307/1785041>.
- Leakey, L.S.B., 1950. The lower limit of the Pleistocene in Africa. *Rep. 18th Int. Geol. Congr. (London)* 62–65.
- Leakey, M.D., Leakey, L.S.B., Game, P.M., Goodwin, A.J.H., 1943. Report on the excavations at Hyrax Hill, Nakuru, Kenya colony, 1937–1938. *Trans. Roy. Soc. S Afr.* 30 (4), 271–409. <https://doi.org/10.1080/00359194309519847>.
- Leat, P.T., 1984. Geological evolution of the trachytic caldera Volcano menengai, Kenya Rift Valley. *J. Geol. Soc.* 141 (6), 1057–1069. <https://doi.org/10.1144/gsjgs.141.6.1057>.
- Levin, N.E., Zipser, E.J., Cerling, T.E., 2009. Isotopic composition of waters from Ethiopia and Kenya: insights into moisture sources for eastern Africa. *J. Geophys. Res.* 114, D23306. <https://doi.org/10.1029/2009JD012166>.
- Livingstone, D.A., Melack, J.M., 1984. Some Lakes of subsaharan Africa. In: Taub, F.B. (Ed.), *Lakes and Reservoirs*, pp. 467–497.
- Lüdecke, H.-J., Müller-Plath, G., Wallace, M.G., Lüning, S., 2021. Decadal and multidecadal natural variability of African rainfall. *J. Hydrol.* 34, 100795. <https://doi.org/10.1016/j.ejrh.2021.100795>.
- Lung’ayia, H., Sitoki, L., Kenyana, M., 2001. The nutrient enrichment of Lake Victoria (Kenyan Waters). *Hydrobiologia* 458 (1–3), 75–82. <https://doi.org/10.1023/A:101312802773>.
- Lupien, R.L., Russell, J.M., Pearson, E.J., Castañeda, I.S., Asrat, A., Foerster, V., Lamb, H.F., et al., 2022. Orbital controls on Eastern African hydroclimate in the Pleistocene. *Sci. Rep.* 12 (1), 3170. <https://doi.org/10.1038/s41598-022-06826-z>.
- MacIntyre, S., Roberts, R.D., Goldman, C.R., Kumagai, C., 2012. Climatic variability, mixing dynamics, and ecological consequences in the African Great Lakes. In: *Climatic Change and Global Warming of Inland Waters*. John Wiley & Sons, Ltd, Chichester, UK, pp. 311–336. <https://doi.org/10.1002/9781118470596.ch18>.
- Mahamat Ahmat, A., Boussafir, M., Le Milbeau, C., Guégan, R., De Oliveira, T., Le Forestier, L., 2017. Organic matter and clay interaction in a meromictic Lake: implications for source rock OM preservation (Lac pavin, Puy-De-Dôme, France). *Org. Geochem.* 109, 47–57. <https://doi.org/10.1016/j.orggeochem.2017.03.014>.
- Marchant, R., Mumbi, C., Behera, S., Yamagata, T., 2007. The Indian Ocean dipole the unsung driver of climatic variability in East Africa. *Afr. J. Ecol.* 45 (1), 4–16. <https://doi.org/10.1111/j.1365-2028.2006.00707.x>.
- Maslin, M.A., Trauth, M.H., 2009. Plio-Pleistocene East African pulsed climate variability and its influence on early human evolution. In: *The First Humans – Origin and Early Evolution of the Genus Homo*. Dordrecht: Springer, Netherlands, pp. 151–158.
- McCall, G.J.H., 1967. *Geology of the Nakuru-thomson's Falls-Lake Hannington Area*. Meyers, P.A., 1994. Preservation of elemental and isotopic source identification of sedimentary organic matter. *Chem. Geol.* 114 (3), 289–302. [https://doi.org/10.1016/0009-2541\(94\)90059-0](https://doi.org/10.1016/0009-2541(94)90059-0).
- Meyers, P.A., 2003. Applications of organic geochemistry to paleolimnological reconstructions: a summary of examples from the Laurentian Great Lakes. *Org. Geochem.* 34, 261–289.
- Milbrink, G., 1977. On the limnology of two alkaline Lakes (Nakuru and Naivasha) in the East Rift Valley System in Kenya. *Int. Rev. Gesamten Hydrobiol.* 62 (1), 1–17. <https://doi.org/10.1002/iqh.1977.3510620101>.
- Moos, M.T., Laird, K.R., Cumming, Brian F., 2005. Diatom assemblages and water depth in Lake 239 (experimental Lakes area, Ontario): implications for Paleoclimatic studies. *J. Paleolimnol.* 34 (2), 217–227. <https://doi.org/10.1007/s10933-005-2382-8>.
- Muiruri, V., Owen, R.B., Potts, R., Deino, A.L., Behrensmeyer, A.K., Riedl, S., Rabideaux, N., et al., 2021. Quaternary diatoms and paleoenvironments of the Koora Plain, Southern Kenya rift. *Quat. Sci. Rev.* 267, 107106. <https://doi.org/10.1016/j.quascirev.2021.107106>.
- Naeher, S., Gilli, A., North, R.P., Hamann, Y., Schubert, C.J., 2013. Tracing bottom water oxygenation with sedimentary Mn/Fe ratios in Lake Zurich, Switzerland. *Chem. Geol.* 352, 125–133. <https://doi.org/10.1016/j.chemgeo.2013.06.006>.
- Ndebele-Murisa, M., Musil, C.F., Raitt, L., 2010. A review of phytoplankton dynamics in tropical African Lakes: review article. *South Afr. J. Sci.* 106 (1), 13–18.
- Nicholson, S.E., 2018. The ITCZ and the seasonal cycle over equatorial Africa. *American Meteorological Society* 337–348. <https://doi.org/10.1175/BAMS-D-16-0287.1>.
- Nicholson, S.E., 2017. Climate and climatic variability of rainfall over Eastern Africa. *Rev. Geophys.* 55 (3), 590–635. <https://doi.org/10.1002/2016RG000544>, 1985.
- Nicholson, S.E., 1996. A review of climate dynamics and climate variability in Eastern Africa. In: Johnson, Thomas C., Odada, Eric O. (Eds.), Whittaker, Katherine T., *The Limnology, Climatology and Paleoclimatology of the East African Lakes*. Gordon and Breach Science Publishers, Amsterdam, pp. 25–56.
- Nilsson, E., 1940. Ancient changes of climate in British East Africa and Abyssinia: a study of Ancient Lakes and glaciers. *Geogr. Ann.* 22 (1–2), 1–79. <https://doi.org/10.1080/20014422.1940.11880682>.
- Nilsson, E., 1931. Quaternary glaciations and pluvial Lakes in British East Africa. *Geogr. Ann.* 13, 249–349. <https://doi.org/10.2307/519647>.
- North Greenland Ice Core Project members, 2004. High-resolution record of northern hemisphere climate extending into the last interglacial period. *Nature* 431, 147–151.
- Ntale, H.K., Gan, T.Y., 2004. East African rainfall anomaly patterns in association with El Niño/Southern oscillation. *J. Hydrol. Eng.* 9 (4), 257–268. [https://doi.org/10.1061/\(ASCE\)1084-0699\(2004\)9:4\(257\)](https://doi.org/10.1061/(ASCE)1084-0699(2004)9:4(257)).
- Nutz, A., Kwiecien, O., Buylaert, J.P., Guihou, A., Khabouchi, I., Deschamps, P., Breitenbach, S.F.M., et al., 2024. A 60–50 Ka African humid period modulated by stadial heinrich events HE6 and HE5a in Northwestern Africa. *Palaeogeogr.*
- Palaeoclimatol. Palaeoecol. 635 (February), 111952. <https://doi.org/10.1016/j.palaeo.2023.111952>.
- Odada, E.O., Raini, J., Ndetei, R., 2006. *Lake Nakuru: Experience and Lessons Learned Brief*.
- Oksanen, J., Blanchet, F.G., Friendly, M., Kindt, R., Legendre, P., McGlinn, D., Minchin, P.R., O’Hara, R.B., Simpson, G.L., Solymos, P., 2022. *Vegan: community ecology package. R Package Version 2, 5–2020*.
- Olaka, L., Odada, E., Trauth, M., Olago, D., 2010. The sensitivity of East African rift Lakes to climate fluctuations. *J. Paleolimnol.* 44 (2), 629–644. <https://doi.org/10.1007/s10933-010-9442-4>.
- O’Mara, Nicholas A., Skonieczny, Charlotte, McGee, David, Winckler, Gisela, Bory, Aloys J.-M., Bradtmiller, Louisa I., Malazé, Bruno, Polissar, Pratigya J., 2022. Pleistocene drivers of Northwest African hydroclimate and vegetation. *Nat. Commun.* 13 (1), 3552. <https://doi.org/10.1038/s41467-022-31120-x>.
- Otto-Blaesner, B., Russell, J.M., Clark, P.U., Liu, Z., Overpeck, J.T., Konecky, B., deMenocal, P., Nicholson, S.E., He, F., Lu, Z., 2014. Coherent changes of Southeastern equatorial and Northern African rainfall during the last deglaciation. *Science* 346 (6214), 1223–1227. <https://doi.org/10.1126/science.1259531>.
- Owen, R.B., Crossley, R., 1992. Spatial and temporal distribution of diatoms in sediments of Lake Malawi, Central Africa, and ecological implications. *J. Paleolimnol.* 7 (1), 55–71. <https://doi.org/10.1007/BF00197031>.
- Owen, R.B., Renaud, R.W., Behrensmeyer, A.K., Potts, R., 2014. Quaternary geochemical stratigraphy of the Kedong-Olorgesailie section of the Southern Kenya Rift Valley. *Palaeogeogr. Palaeoclimatol. Palaeoecol.* 396, 194–212. <https://doi.org/10.1016/j.palaeo.2014.01.011>.
- Pilskaln, C.H., 2004. Seasonal and interannual particle export in an African rift Valley Lake: a 5-Yr record from Lake Malawi, Southern East Africa. *Limnol. Oceanogr.* 49 (4), 964–977. <https://doi.org/10.4319/lo.2004.49.4.0964>.
- Pilskaln, C.H., Johnson, T.C., 1991. Seasonal signals in Lake Malawi sediments. *Limnol. Oceanogr.* 36 (3), 544–557. <https://doi.org/10.4319/lo.1991.36.3.0544>.
- Porter, S.C., Zhisheng, A., 1995. Correlation between climate events in the North Atlantic and China during the last glaciation. *Nature (London)* 375 (6529), 305–308. <https://doi.org/10.1038/375305a0>.
- Potts, R., 1998. Environmental hypotheses of Hominin evolution. *Am. J. Phys. Anthropol.* 107 (27), 93–136. [https://doi.org/10.1002/\(SICI\)1096-8644\(1998\)107:27+3.0.CO;2-X](https://doi.org/10.1002/(SICI)1096-8644(1998)107:27+3.0.CO;2-X).
- RCMRD, 2021. *The Rising Water Level and Expansion of the Rift Valley Lakes from Space. Nairobi, Kenya*.
- Reimer, P.J., Austin, W.E.N., Bard, E., Bayliss, A., Blackwell, P.G., Ramsey, C.B., Butzin, M., et al., 2020. The IntCal20 Northern hemisphere radiocarbon age calibration curve (0–55 cal kBP). *Radiocarbon* 62 (4), 725–757. <https://doi.org/10.1017/RDC.2020.41>.
- Renaud, R.W., Owen, R.B., 2023. The central Kenya rift basins (Nakuru-Elementaita-Naivasha). In: *The Kenya Rift Lakes: Modern and Ancient. Syntheses in Limnogeology*. Springer, Berlin, Heidelberg. https://doi.org/10.1007/978-3-642-25055-2_18.
- Renaud, R.W., Owen, R.B., Lowenstein, T.K., De Cort, G., Mcnulty, E., Scott, J.J., Mbuthia, A., 2021. The role of hydrothermal fluids in sedimentation in saline alkaline lakes: evidence from Nasikie Engida, Kenya Rift Valley. *Sedimentology* 68, 108–134. <https://doi.org/10.1111/sed.12778>.
- Richardson, J.L., Dussinger, R.A., 1986. Paleolimnology of mid-elevation Lakes in the Kenya rift Valley. *Hydrobiologia* 143 (1), 167–174. <https://doi.org/10.1007/BF00266559>.
- Richardson, J.L., Richardson, A.E., 1972. History of an African rift Lake and its climatic implications. *Ecol. Monogr.* 42 (4), 499–534.
- Richter, T.O., van der Gaast, S., Koster, B., Vaars, A., Gieles, R., de Stigter, H.C., de Haas, H., van Weering, T.C.E., 2006. The avaaite XRF core scanner: technical description and applications to NE Atlantic sediments. In: Rothwell, R.G. (Ed.), *New Techniques in Sediment Core Analysis*. Geological Society of London, pp. 1–2.
- Robson, G.E., 1967. The Caves of Sof Omar. *Geogr. J.* 133 (3), 344–349. <https://doi.org/10.2307/1793545>.
- Roessner, S., Strecker, M.R., 1997. Late Cenozoic tectonics and denudation in the Central Kenya Rift: quantification of long-term denudation rates. *Tectonophysics* 278, 83–94.
- Roubeix, V., Chalié, F., Gasse, F., 2014. The diatom Thalassiosira Faurii(Gasse) Hasle in the ziway-shala Lakes (Ethiopia) and implications for paleoclimate reconstructions: case Study of the glacial-holocene transition in East Africa. *Palaeogeogr. Palaeoclimatol. Palaeoecol.* 402, 104–112. <https://doi.org/10.1016/j.palaeo.2014.03.014>.
- Ryves, D.B., Juggins, S., Fritz, S.C., Battarbee, R.W., 2001. Experimental diatom dissolution and the quantification of microfossil preservation in sediments. *Palaeogeogr. Palaeoclimatol. Palaeoecol.* 172 (1), 99–113. [https://doi.org/10.1016/S0031-0182\(01\)00273-5](https://doi.org/10.1016/S0031-0182(01)00273-5).
- Sachs, J.P., Lehman, S.J., 1999. Subtropical North Atlantic temperatures 60,000 to 30,000 years ago. *Science* 286 (5440), 756–759. <https://doi.org/10.1126/science.286.5440.756>.
- Schaebitz, F., Asrat, A., Lamb, H.F., Cohen, A.S., Foerster, V., Duesing, W., Kaboth-Bahr, S., et al., 2021. Hydroclimate changes in Eastern Africa over the past 200,000 years may have influenced early human dispersal. *Commun. Earth Environ.* 2 (1). <https://doi.org/10.1038/s43247-021-00195-7>.
- Shakun, Jeremy D., Carlson, Anders E., 2010. A global perspective on last glacial maximum to Holocene climate change. Special Theme: Arctic Palaeoclimate Synthesis 29 (15), 1801–1816. <https://doi.org/10.1016/j.quascirev.2010.03.016>, 1674–1790.
- Shanahan, Timothy M., McKay, Nicholas P., Hughen, Konrad A., Overpeck, Jonathan T., Otto-Blaesner, Bette, Heil, Clifford W., King, John, Scholz, Christopher A.,

- Peck, John, 2015. The time-transgressive termination of the African humid period. *Nat. Geosci.* 8 (2), 140–144. <https://doi.org/10.1038/ngeo2329>.
- Singarayer, J.S., Burrough, S.L., 2015. Interhemispheric dynamics of the African rainbelt during the late Quaternary. *Quat. Sci. Rev.* 124, 48–67. <https://doi.org/10.1016/j.quascirev.2015.06.021>.
- Spaulding, S.A., Bishop, L.W., Edlund, M.B., Lee, S., Furey, P., Jovanovska, E., Potapova, M., Diatoms of North America. <https://diatoms.org/species>.
- Stager, J.C., 1988. Environmental Changes at Lake Chesi, Zambia since 40,000 years B.P. *Quat. Res.* 29 (1), 54–65. [https://doi.org/10.1016/0033-5894\(88\)90071-3](https://doi.org/10.1016/0033-5894(88)90071-3).
- Stager, J.C., Mayewski, Paul A., Meeker, L.D., 2002. Cooling cycles, heinrich event 1, and the desiccation of Lake Victoria. *Palaeogeogr. Palaeoclimatol. Palaeoecol.* 183 (1–2), 169–178. [https://doi.org/10.1016/S0031-0182\(01\)00468-0](https://doi.org/10.1016/S0031-0182(01)00468-0).
- Stager, J.C., Ryves, D.B., Chase, B.M., Pausata, F.S.R., 2011. Catastrophic drought in the Afro-Asian monsoon Region during heinrich event 1. *Science*. <https://doi.org/10.1126/science.1198322>.
- Stevenson, R.J., Stoermer, E.F., 1981. Quantitative differences between benthic algal communities along a depth gradient in Lake Michigan. *J. Phycol.* 17 (1), 29–36. <https://doi.org/10.1111/j.1529-8817.1981.tb00815.x>.
- Strecker, M.R., Blisniuk, P.M., Eisbacher, G.H., 1990. Rotation of extension direction in the central Kenya rift. *Geology (Boulder)* 18 (4), 299–302. [https://doi.org/10.1130/091-7613\(1990\)0182.3.CO;2](https://doi.org/10.1130/091-7613(1990)0182.3.CO;2).
- Talling, J.F., 2001. Environmental controls on the functioning of shallow tropical Lakes. *Hydrobiologia* 458 (1–3), 1–8. <https://doi.org/10.1023/A:1013121522321>.
- Taylor, J.C., Cocquyt, C., 2016. Diatoms from the Congo and Zambezi Basins – Methodologies and Identification of the Genera, 44. Informa UK Limited. <https://doi.org/10.2989/16085914.2019.1628702>.
- Taylor, J.C., Harding, W.R., Archibald, C.G.M., 2007. An illustrated guide to some common diatom species from South Africa. Pretoria, South Africa: Water Research Commission.
- ter Braak, C., Looman, C., 1986. Weighted averaging, logistic regression and the gaussian response model. *Vegetatio* 65 (1), 3–11. <https://doi.org/10.1007/BF00032121>.
- Thevenon, F., Williamson, D., Taieb, M., 2002. A 22 Kyr BP sedimentological record of Lake Rukwa (8°S, SW Tanzania): environmental, chronostratigraphic and climatic implications. *Palaeogeogr. Palaeoclimatol. Palaeoecol.* 187 (3), 285–294. [https://doi.org/10.1016/S0031-0182\(02\)00481-9](https://doi.org/10.1016/S0031-0182(02)00481-9).
- Tian, Z., Jiang, D., 2020. Weakening and eastward shift of the tropical Pacific walker circulation during the last glacial maximum. *Boreas* 49 (1), 200–210. <https://doi.org/10.1111/bor.12417>.
- Tierney, J., deMenocal, P., 2013. Abrupt shifts in horn of Africa hydroclimate since the Last Glacial Maximum. *Science* 342 (6160), 843–846. <https://doi.org/10.1126/science.1240411>.
- Tierney, J.E., Russell, J.M., Huang, Y., Sinnunghe Damsté, J.S., Hopmans, E.C., Cohen, A. S., 2008. Northern hemisphere controls on tropical Southeast African climate during the past 60,000 years. *Science (New York, N.Y.)* 322 (5899), 252. <https://doi.org/10.1126/science.1160485>.
- Tierney, J.E., Russell, J.M., Sinnunghe Damsté, Huang, Y., Verschuren, D., 2011. Late Quaternary behavior of the East African monsoon and the importance of the Congo Air Boundary. *Quat. Sci. Rev.* 30, 798–807. <https://doi.org/10.1016/j.quascirev.2011.01.017>.
- Tjallingii, R., Claussen, M., Stuut, J.B.W., Fohlmeister, J., Jahn, A., Bickert, T., Lamy, F., Röhl, U., 2008. Coherent High- and low-latitude control of the Northwest African hydrological balance. *Nat. Geosci.* 1 (10), 670–675. <https://doi.org/10.1038/ngeo289>.
- Trauth, M.H., Deino, A.L., Bergner, A.G.N., Strecker, M.R., 2003. East African climate change and orbital forcing during the last 175 kyr BP. *Earth Planet. Sci. Lett.* 206, 297–313. [https://doi.org/10.1016/S0012-821X\(02\)01105-6](https://doi.org/10.1016/S0012-821X(02)01105-6).
- Trauth, M.H., Foerster, V., Junginger, A., Asrat, A., Lamb, H.F., Schaebitz, F., 2018. Abrupt or gradual? Change point analysis of the late Pleistocene–Holocene climate record from Chew Bahir, Southern Ethiopia. *Quat. Res.* 90 (2), 321–330. <https://doi.org/10.1017/qua.2018.30>.
- Trauth, M.H., Maslin, M.A., Deino, A.L., Junginger, A., Lesoloyia, M., Odada, E.O., Olago, D.O., Olaka, L.A., Strecker, M.R., Tiedemann, R., 2010. Human evolution in a variable environment: the amplifier Lakes of Eastern Africa. *Quat. Sci. Rev.* 29 (23), 2981–2988. <https://doi.org/10.1016/j.quascirev.2010.07.007>.
- Truc, L., Chevalier, M., Favier, C., Cheddadi, R., Meadows, M.E., Scott, L., Carr, A.S., Smith, G.F., Chase, B.M., 2013. Quantification of climate change for the last 20,000 years from wonderkrater, South Africa: implications for the long-term dynamics of the intertropical convergence zone. *Palaeogeogr. Palaeoclimatol. Palaeoecol.* 386, 575–587. <https://doi.org/10.1016/j.palaeo.2013.06.024>.
- Vareschi, E., Jacobs, J., 1985. The ecology of Lake Nakuru. VI. Synopsis of production and energy flow. *Oecologia* 65 (3), 412–424. <https://doi.org/10.1007/BF00378917>.
- Verschuren, D., Sinnunghe Damsté, J.S., Moernaut, J., Kristen, I., Blaauw, M., Fagot, M., Haug, H.G., et al., 2009. Half-precessional dynamics of monsoon rainfall near the East African equator. *Nature (London)* 462 (7273), 637–641. <https://doi.org/10.1038/nature08520>.
- Voelker, A.H.L., 2002. Global distribution of centennial-scale records for Marine Isotope Stage (MIS) 3: a database. *Quat. Sci. Rev.* 21 (10), 1185–1212. [https://doi.org/10.1016/S0277-3791\(01\)00139-1](https://doi.org/10.1016/S0277-3791(01)00139-1).
- Wang, Y.J., Cheng, H., Edwards, R.L., An, Z.S., Wu, J.Y., Shen, C.-C., Dorale, J.A., 2001. A high-resolution absolute-dated late Pleistocene monsoon record from Hulu Cave, China. *Science* 294 (5550), 2345–2348. <https://doi.org/10.1126/science.1064618>.
- Washbourn-Kamau, C.K., 1971. Late Quaternary Lakes in the Nakuru-Elmenteita Basin, Kenya. *Geogr. J.* 137 (4), 522–535. <https://doi.org/10.2307/1797148>.
- Wienhues, G., Temoltzin-Loranca, Y., Vogel, H., Morlock, M.A., Cohen, A.S., Anselmetti, F.S., Bernasconi, S.M., Jaggi, M., Tylmann, W., Kishe, M.A., King, L., Ngoepe, N., Courtney-Mustaphi, C.J., Muschick, M., Matthews, B., Mwaiko, S., Seehausen, O., Tinner, W., Grosjean, M., 2023. From desiccation to wetlands and outflow: rapid re-filling of Lake Victoria during the Latest Pleistocene 14–13 ka. *J. Great Lake Res.*, 102246 <https://doi.org/10.1016/j.jglr.2023.102246>.
- Yuan, W., Liu, G., Xu, L., Niu, X., Li, C., 2019. Petrographic and geochemical characteristics of organic-rich shale and tuff of the Upper Triassic Yanchang Formation, Ordos Basin, China; implications for lacustrine fertilization by volcanic ash. *Can. J. Earth Sci.* 56 (1), 47–59. <https://doi.org/10.1139/cjes-2018-0123>.
- Yuretich, R.F., 1982. Possible influences upon Lake development in the East African rift Valleys. *J. Geol.* 90 (3), 329–337. <https://doi.org/10.1086/628684>.
- Zébazé Togouet, S.H., Njine, T., Kemka, N., Nola, M., Menbohan, S.F., Koste, W., Boutin, C., Hochberg, R., 2007. Spatio-temporal changes in the abundance of the populations of the gastrotrich community in a Shallow Lake of Tropical Africa. *Limnologica* 37 (4), 311–322. <https://doi.org/10.1016/j.limno.2007.06.003>.
- Zeileis, A., Grothendieck, G., 2005. Zoo : S3 infrastructure for regular and irregular time series. *J. Stat. Software* 14 (6). <https://doi.org/10.18637/jss.v014.i06>.
- Zielke, O., Strecker, M.R., 2009. Recurrence of large earthquakes in magmatic Continental rifts: insights from a paleoseismic study along the laikipia–marmarant fault, Subukia Valley, Kenya rift. *Bull. Seismol. Soc. Am.* 99 (1), 61–70. <https://doi.org/10.1785/0120080015>.